Sustainable Energy Technologies and Assessments 51 (2022) 101941

Contents lists available at ScienceDirect

Sustainable Energy Technologies and Assessments

journal homepage: www.elsevier.com/locate/seta

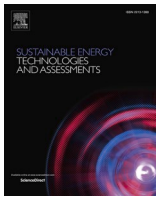

Original article

Enhancing the thermal efficiency of parabolic trough collector using rotary receiver tube

N. Sreenivasalu Reddy [a,*], S. Gowreesh Subramanya [b], K.C. Vishwanath [a], M. Karthikeyan [a], S. Kanchiraya [c]

[a] Department of Mechanical Engineering, RajaRajeswari College of Engineering, Bengaluru 560074, Karnataka, India
[b] Department of Mechanical Engineering, JSS Academy of Technical Education, Bengaluru 560060, Karnataka, India
[c] Department of Mechanical Engineering, Government Engineering College, Hassan 573201, Karnataka, India

ARTICLE INFO

Original content: https://doi.org/10.1016/j.enconman.2014.09.056

Keywords:
Rotary receiver tube
Heat transfer enhancement
Thermal efficiency
Friction factor

ABSTRACT

The performance of the parabolic trough collector is studied experimentally using a rotary receiver tube. The parameters such as temperature increase, friction factor and thermal efficiency at receiver tube speed of 0, 2 and 4 rpm are investigated. Tests were performed for varied inlet temperatures and flow rates. From the achieved results, it is found that the friction factor increases dramatically due to the usage of rotary receiver tube. Furthermore, for receiver tube speeds of 4, 2 and 0 rpm the maximum values of temperature differences are found to be 18.5 °C, 12.5 °C and 4.0 °C respectively. It is found that the enhancement of the thermal efficiency is due to decreasing the inlet temperature and by increasing the flow rate. Moreover, the highest thermal efficiency improvement of the collector is due to the usage of rotary receiver tube. Maximum efficiency improvement for a tube speed of 4 and 2 rpm is found to be 190.3% and 158.6% respectively in comparison with the stationary receive tube.

Introduction

Solar energy is a good alternative for fossil fuel depletion and environmental impacts [1–3]. Parabolic trough collectors (PTC) can produce high-temperature levels; hence, PTC can be used in many applications such as industrial cooling, refrigeration system, desalination and power generation [4,5].

PTC is one of the common focused technologies [6,7], a solar field with PTC occupying 2000 m^2 to generate a power of 1 MW. In recent years, a lot of research has been focused on thermal efficiency improvement to generate a useful amount of heat. Techniques are needed to enhance the thermal efficiencies, the main aim of these techniques is to minimize the thermal stresses and possibility of failure [8].

In one of the techniques, the usage of inserts and nanofluids leads to improvements in the performance of the PTC. In general, nanofluids consists of two fluids, one fluid (fluid of nanometers) is diffused with another (water or oil) in order to augment the fluid thermal conductivity [9]. The usage of nanofluids leads to progress the performance of the PTC. However, some of the difficulties in dealing with nanofluids are its high cost and the problems due to stability. The difficulties faced in dealing with nanofluids are as they are high cost and due to their stability problem [10]. The better way of selecting the nanofluid is the use of right surfactants and the other technique is the usage of inserts; wherein the geometry of the inner tube of receiver is modified. The main idea is to create vortices, which leads to better mixing and turbulence [11].

The outcome is to increase the performance of the PTC. In particular, the heat transfer coefficient increases when the receiver tube temperature reduces, obviously thermal efficiency increases. The disadvantage of using inserts leads to rise in frictional resistance. It is clear from the literature that there are more investigations have been carried out on the modification of geometry of the receiver tube of PTC.

Bellos et al. [12] investigated the enhancement of thermal efficiency by means of converging–diverging turbulators in the receiver tube and found that increase in thermal efficiency by 5% as compared to plain tube. Fuqiang et al. [13] studied a corrugated receiver tube and noticed that the Nusselt number is raised by 53 % as compared to bare tube at the cost of pumping power by 15%. Huang et al. [14] shown that the pit type receiver tube enhances the fluid film coefficient by around 38%.In another work, Bitam et al. [15] analyzed thermal efficiency,

* Corresponding author.
E-mail address: nsreddysrsit@gmail.com (N. Sreenivasalu Reddy).

https://doi.org/10.1016/j.seta.2021.101941
Received 31 August 2021; Received in revised form 15 November 2021; Accepted 23 December 2021
Available online 5 January 2022

Nomenclature

A	Area (m^2)
C_p	Specific heat (J/kg °C)
G	Normal solar irradiation on aperture (W/m^2)
T	temperature (°C)
$\dot{m}$	Mass flow rate (kg/s)
P	Pressure (Pa)
d	Diameter of receiver glass (mm)
f	Friction factor
lph	Litres per hour
rpm	Revolutions per hour

Subscripts

i	Inlet
o	outlet
ap	Aperture
ss	steady-state
col	Collector

Greek symbols

ρ	density of fluid (kg/m^3)
η	Collector efficiency (%)

temperature and friction factor and found that there is 60% raise in heat transfer coefficient and 3% collector efficiency at a cost of 50% raise in pressure drop. Many of the researchers have been investigated mainly on the geometry of the receiver tube since as the surface area increases solar heat flux also increases. Cheng et al. [16] proved that swirl generators in the receiver tube causes better fluid film coefficient nearer to 65% and raises the pumping power by 2.5 times more as that of smooth tube. Furthermore, Xiangtao et al. [17] verified the arrangement of fins on the circumference of the receiver tube and achieved the Nusselt number by 3%. Benabderrahmane et al. [18] studied the thermal characteristics, enhancement of heat transfer and friction factor on the longitudinal fins and found that there is a raise in pressure drop by 60% and film coefficient by 70%.

Moreover, Reddy et al. [19] investigated longitudinal fins by using the porous media in the receiver tube and found that the increase of film effectiveness by 40% and the pumping power increases by 1.2 times in comparing with smooth tubes. Munoz et al. [8,20] studied the thermal efficiency by using helical fins and found that increase in thermal efficiency by 2%. Bellos et al. [21–24] studied the internal fins on the outer circumference of the receiver tube. The study on the use of extended surfaces are the another area of research in the literature. Aramilloet et al. [25] investigated the use of flow inserts in the receiver tube of PTC and achieved that the efficiency of the collector was augmented by 10%. Mwesigye et al. [26] investigated the overall heat transfer coefficient and enhanced 7 times as compared to receiver tube without inserts. Ghadirijafarbeigloo et al. [27] examined leafy shaped twisted insert at different angles and found that the film coefficient was doubled. Furthermore, Rawani et al. [28] examined that the usage of inserts with different pitch ratios increases the fluid film coefficient by 3.5 times, as that of receiver tube without inserts.

Another researcher Chang et al. [29] studied that there is a rise in heat transfer rate by 200% as compared with a conventional tape inserts. The same ideas have been applied by some other researchers by using wave type insert [30], helical tape inserts with different pitch ratios [31] and double bended tape inserts [32]. Furthermore, Divan et al. [33] and Sahin et al. [34] studied the enhancement of heat transfer on wire coils. Both of these studies explain that there is a raise in heat transfer coefficient by 300%, which is about twenty times more as compared with plain tube. Jamal-Abad et al. [35] investigated the use of metal inserts and found that the enhancement of collector efficiency was about 3.5%, and the pumping power was 20 times larger than that of receiver tube without inserts. Wang et al. [36] studied the pressure drop and film coefficient and the results showed that there is a raise in heat transfer coefficient by 7 times greater than that of reference case. Mwesigye et al. [37,38] studied the performance of PTC and found that the efficiency enhancement by 8% and the raise in pressure drop by 25 times. Chang et al. [39] investigated the use of spherical shape coils and achieved the heat transfer coefficient of 600% and at a cost of pressure drop 10 times more. Furthermore, Bellos et al. [40] studied the star shaped inserts and found that the enhancement of the thermal efficiency is up to 1% and frictional resistance increased from 200% to 800%.

Some of the researchers studied the use of porous disc. Ghasemi and Ranjbar [5] examined the thermal efficiency and friction factor by using porous disc and they found film coefficient enhances 50% and pumping power increased by 10 times. Kumar and Reddy [41] achieved the film coefficient of 65% and pressure drop of 15 times. In addition, Reddy et al. [42] studied the same methodology and found raise in collector efficiency by 7%. Zheng et al. [43] investigated the thermal efficiency by using the steam and porous discs and found that there is an improvement in efficiency by 3%.Moreover, some of the researchers carried out the comparative studies. Too and Benito [44] studied the comparison of dimpled, tape inserts and coils and they found that the use of dimple technique is the best.

Mario Biencinto et al. [45] developed a new concept that uses a large aperture area with molten salt as a storage medium. The proposed model achieved a thermal efficiency of 0.5% more in comparison with reference solar power plant. Anil Kumar et al. [46] studied the performance of parabolic trough collector with single slope solar still and obtained an increase in daily water production as compared with conventional solar still. Shaobing Wu et al. [47] developed a novel algorithm to evaluate the intercept factors of parabolic trough collector using a python program and incorporated a secondary mirror design.

Due to the lack of study on rotary receiver tube of PTC, the present study aims to propose a novel parabolic trough collector by providing rotary motion to the receiver tube. The idea of the present work is to examine experimentally, the influence of rotary motion on the performance of the PTC. A parabolic trough collector was designed and developed in order to study the influence of rotary motion on outlet temperature, thermal efficiency and pressure drop. In the present work, the thermal efficiency, friction factor and temperature difference for parabolic trough collector are evaluated at different speeds (0 rpm, 2 rpm and 4 rpm) of the receiver tube.

Material and methods

Test facility

The test facility consists of supporting structure, receiver tube, cooling system, reflector and water tank. A reflector of thickness 1 mm was made with steel mirror. The specification of the collector is; aperture width of 0.7 m, length of 1.5 m, rim angle of $90^o$and focal length of 0.174 m (Table 1. The calculations of dimensions are referred by

Table 1
Specifications of mirror reflector.

Parabola Length (m)	1.5
Width of the aperture (m)	0.7
Area of the aperture (m^2)	0.98
Focal distance (m)	0.174
Angle of the rim	90^0
Thickness of the reflector (mm)	1
Internal diameter of the receiver tube (mm)	22
External diameter of the receiver tube (mm)	26
Inner diameter of the glass cover (mm)	50
Outer diameter of the glass cover (mm)	60
Length of tubes (m)	1.4

Kasaeian [48].

Components of rotating receiver tube and their design

Fig. 1 shows Three-dimensional view of parabolic trough solar energy collector with rotary receiver tube. Figs. 2 and 3 shows the front view and Sectional side view of parabolic trough solar energy collector with rotary receiver tube. The rotating receiver tube assembly consists of housing, inlet pipe, outlet pipe, flywheel, flywheel-shaft, spacers, circular clips and bearings. The spacers were used to maintain the space between the tube support structure and the respective component and helps in making the receiver tube to rotate uniformly. Circular clips were used to support and hold the bearings in its right place. The fabricated rotating receiver tube is as shown in Fig. 4. The materials used in the manufacturing of PTC are listed out in Table 2.

Test rig and instrument

In order to study the performance of the PTC with rotary receiver tube, ASHRAE standard 93-2010 [49] is used. The experiments were conducted on different speeds of receiver tube that is at 0 rpm, 2 rpm and 4 rpm. The Test facility is shown in Fig. 5. The allowed maximum variation of error of measuring instruments is tabulated in Table 3. All the thermocouples were calibrated and the deviation of error was approximately 0.1 °C. The pressure drop across inlet and outlet of the PTC was measured with the help of differential pressure transmitter. The differential pressure transmitter was calibrated and the error found to be ±2 Pa. In order to measure flow rate, a flow meter was used with a range of 20–80 lph. The flow meter was calibrated using a standard beaker method with a deviation of 1% error. The temperature of working fluid was controlled by a cooling system in the range of 20 °C to 40 °C and a pump was used to pump the water in the receiver tube.

Data deduction and uncertainty analysis

Collector efficiency is evaluated by experimental data as per the Eq. (1) as follows:

$$\eta_{col} = \frac{\dot{m}c_p(T_o - T_i)}{A_{ap}G_{ap}} \tag{1}$$

where $\dot{m}$ is the mass flow rate of the fluid, c_p is the specific heat of the working fluid, T_o is the temperature of water at outlet, T_i is the temperature of water at inlet, A_{ap} is the area of the aperture and G_{ap} denotes the solar irradiance.

Friction factor is evaluated according to the Eq. (2) as follows:

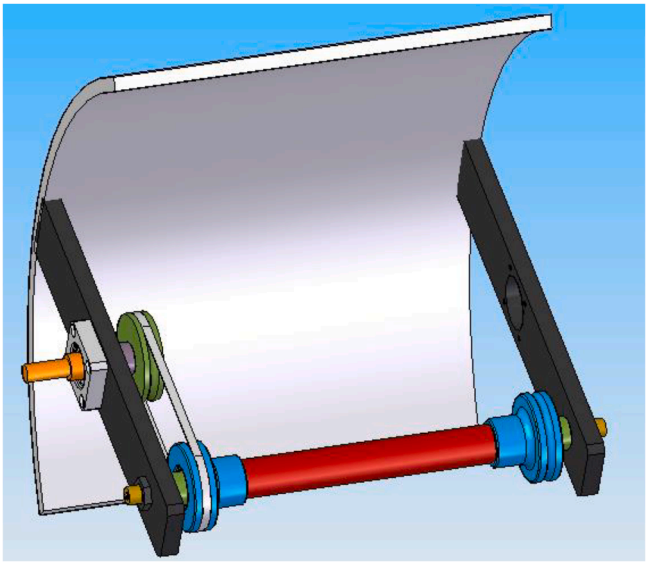

Fig. 1. Three-dimensional view of parabolic trough solar energy collector with rotary receiver tube.

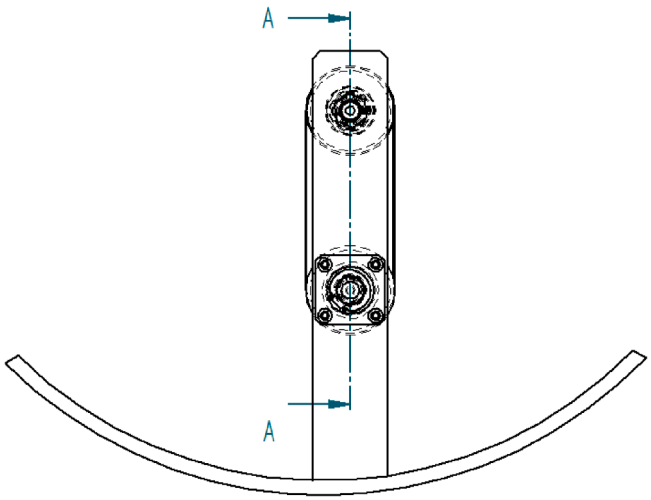

Fig. 2. Front view of parabolic trough solar energy collector with rotary receiver tube.

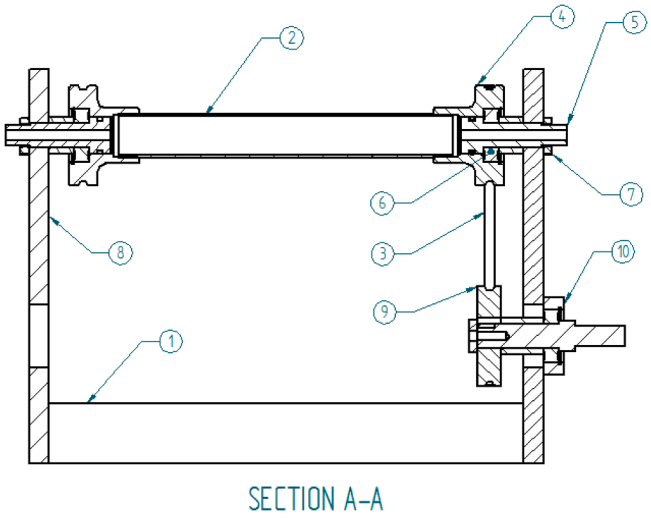

Fig. 3. Sectional side view of parabolic trough solar energy collector with rotary receiver tube.

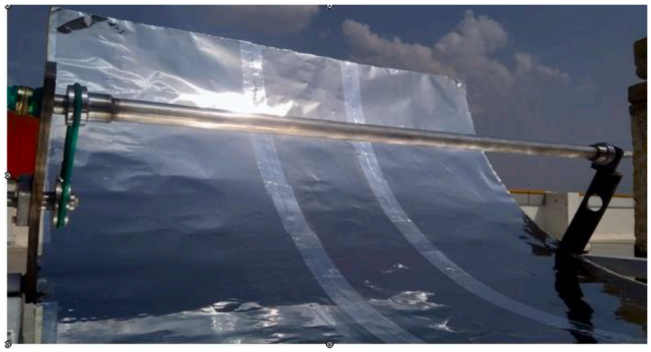

Fig. 4. Fabricated parabolic trough collector with rotary receiver tube.

Table 2
Materials used in the manufacturing of PTC.

Name of the component	Material used
Reflector	Steel mirror
Fixtures	Polyglass
bushing	Polyethylene
Receiver tube	Copper
Belt	Leather
Bearing	silicon Nitride
Nut	Steel
Fly wheel	Mild Steel
Flywheel housing	Stainless Steel

$$f = \frac{\Delta P}{\left(\frac{L}{d}\right)\left(\frac{\rho U^2}{2}\right)} \tag{2}$$

where ΔP is the pressure difference across the collector, L is the length of the absorber tube, d is the diameter of the absorber tube and U is the mean velocity of the water.

Table 4 shows the values of uncertainty in temperature, flow rate, length of the receiver tube, and diameter and pressure drop of the tube. These values are used to evaluate the uncertainties of friction factor and thermal efficiency. In order to evaluate the pressure drop and thermal efficiency, the uncertainty for the above parameters is given by the Eqs. (3) and (4) as follows [28]:

$$U_\eta = \left(\left(\frac{\partial \eta}{\partial \dot{m}} U_{\dot{m}}\right)^2 + +\left(\frac{\partial \eta}{\partial (A_G)} U_{A_G}\right)^2 + \left(\frac{\partial \eta}{\partial (T_{(m,i)} - T_{(m,o)})} U_T\right)^2 + \left(\frac{\partial \eta}{\partial (G)} U_G\right)^2 \right)^{0.5} \tag{3}$$

$$U_f = \left(\left(\frac{\partial f}{\partial \dot{m}} U_{\dot{m}}\right)^2 + \left(\frac{\partial \eta}{\partial d} U_d\right)^2 + \left(\frac{\partial f}{\partial \Delta P} U_{\Delta P}\right)^2 + \left(\frac{\partial f}{\partial (L)} U_L\right)^2 \right)^{0.5} \tag{4}$$

The values of uncertainties for friction factor and efficiency were 2.52 % and 2.16 %, respectively.

Results and discussion

A receiver tube is supported by a double-sided housing component with sealed bearing, circular clip, inlet/outlet pipe and it holds a reflector mirror, which supports the belt drive coupled with a flywheel. Housing plays a vital role in transferring the working fluid from one end to the other through the main receiver tube. Flywheel coupled with a driven shaft is connected with a belt drive, which helps in rotating the receiver tube. In this connection, a PTC with rotary receiver tube was constructed and its temperature variation, thermal performance and pressure drop was evaluated. The experiments were carried out by varying inlet temperature, mass flow rates and speed of the receiver tube

The performance tests were conducted on February 2021 in Bangalore, (12.9716 °N latitude, 77.5946 °E longitude) Karnataka, India. Tests were conducted to study the influence of volume flow rates in the receiver tubes and at different speeds.

All the experiments were carried out at the time between 11am to 2 pm, in order to achieve transient condition. Time constant of the collector is obtained by following the ASHRAE 93–2010. Time constant is the one of the key parameter to evaluate steady state time. The time constant is evaluated from Eq. (5) as follows

$$T_o - T_i = 0.632\ \left(T_{ss,o} - T_i\right) \tag{5}$$

where Ti & To are the temperature at inlet and outlet respectively, during each time step, Tss,o is steady state temperature at outlet. Fig. 6

Table 3
Maximum allowed Variation of key variables.

Measuring instrument	Accuracy
thermocouples	± 0.1 °C
differential pressure transmitter	± 2 Pa
flow meter (lph)	1%
Solar Power Meter (W/m^2)	± 31

Table 4
Measurement uncertainties from a specific data point.

Variable	Unit	Quantity	Uncertainty
Temperature	°C	2	0.1 °C
Mass flow rate	Kg per s	1	±4%
Pressure drop	Pa	2	±2.5%
Length	m	1	±0.001 m
Diameter	m	1	±0.00001 m

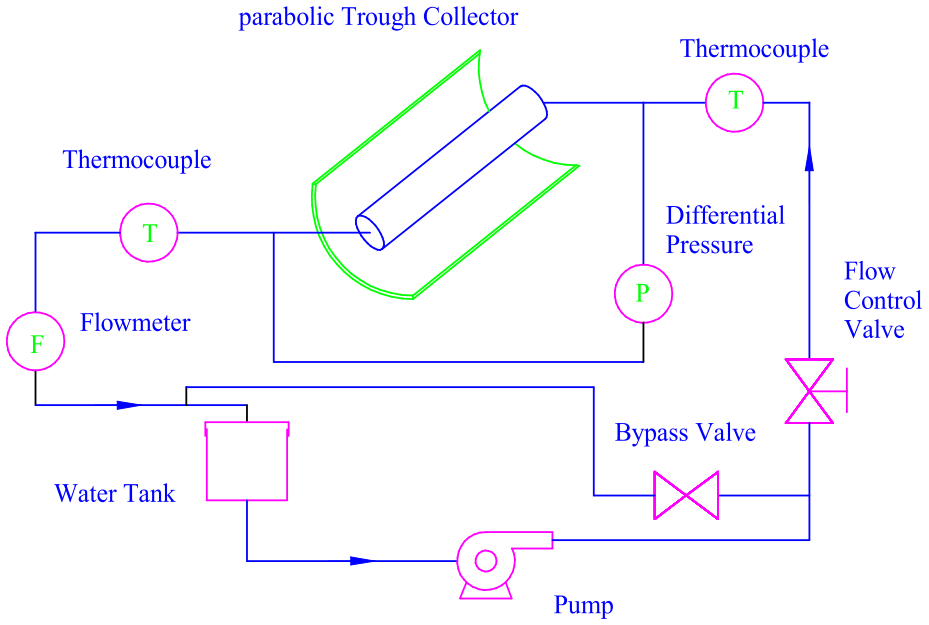

Fig. 5. Schematic of closed loop parabolic trough collector.

shows the temperature rise of water with reference to time. As per the experimental data and Eq. (5), time constant found to be 5.93 min.

Pressure drop

Eq. (2) is used to measure friction factor for different speeds of the receiver tube. Fig. 8 displays friction factor versus Reynolds Number. The results of experiments are validated with theoretical values according to Eqs. (2) and (6) [5].

$$\frac{\Delta P}{\frac{1}{2}\rho U^2} = 13.74\left(\frac{x}{(d.Re)}\right)^{0.5} + \frac{\left(1.25 + 64\left(\frac{x}{(d.Re)} - 13.74(x/(d.Re)\right)^{0.5}\right)}{\left(1 + 0.00021\left(\frac{x}{(d.Re)}\right)\right)^{-2}\right)} \quad (6)$$

Fig. 7 shows the validation of the present values with the available data in the literature [50], and shows good agreement of accuracy. It is very clear from the Fig. 8 that at any particular Reynolds number there is an increase in friction factor as the speed of the receiver tube increases. The results also reveal that at a speed of 4 rpm and 2 rpm there is an increase in the friction factor by 137.5 and 62.5times respectively in compared with stationary tube. Moreover, comparison between experimental data and theoretical values shows good agreement of accuracy for experimental work.

Thermal efficiency

In this section, the influence of various speeds on temperature at inlet and outlet, flow rate and thermal efficiency of a collector are studied. Figs. 9–11 shows temperature of water at outlet and inlet of receiver tube verses mass flow rates of working fluid. It is clear from the Figs. 9–11 that the difference in outlet and inlet temperature is reduced by raising the mass flow rate of the working fluid. In order to evaluate the influence of various speeds (2 rpm and 4 rpm) of receiver tube on thermal efficiency of the collector, the stationary receiver tube (0 rpm) was also tested and its performance was observed. Fig. 9 represents the results of stationary receiver tube at different mass flow rates of working fluid. The results show that rise of minimum and maximum temperature of 1.75 °C and 4 °C respectively. The augments are due to the maximum and minimum mass flow rates of working fluid, respectively. The reason for the augmentation of temperature difference is due to the consumption of time to absorb solar energy is more at low mass flow rate. By using rotary receiver tube, fluid gets better mixing and improves the fluid film coefficient. Fig. 10 shows temperature difference, inlet and outlet temperature of water at 2 rpm. The values of maximum and minimum temperature differences are 12 °C and 8°C at 20 lph and 100

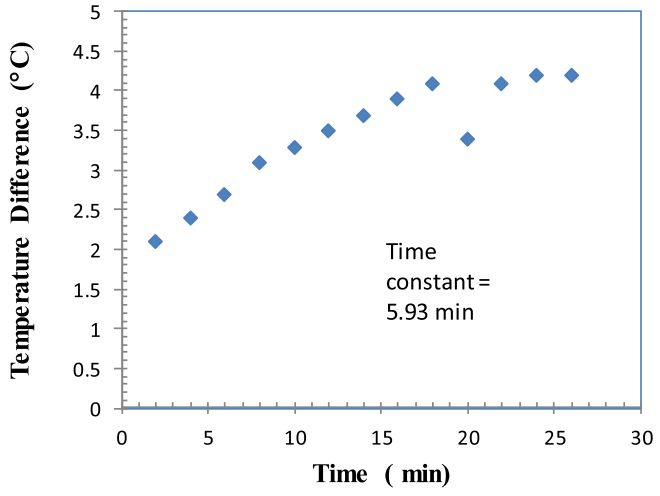

Fig. 6. Variation of temperature difference versus time constant of fabricated collector.

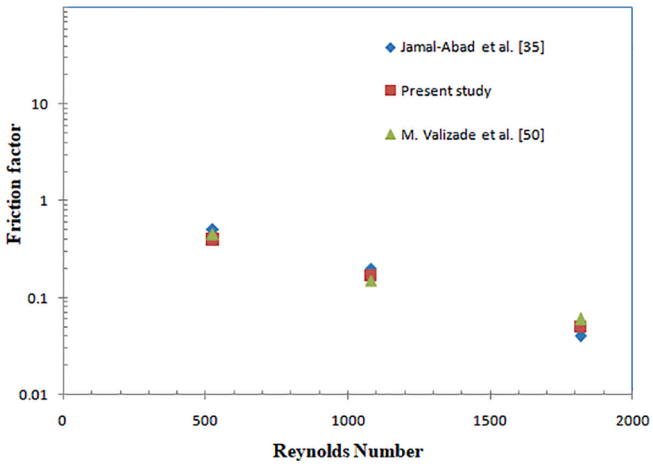

Fig. 7. Variation of friction factor with Reynolds number.

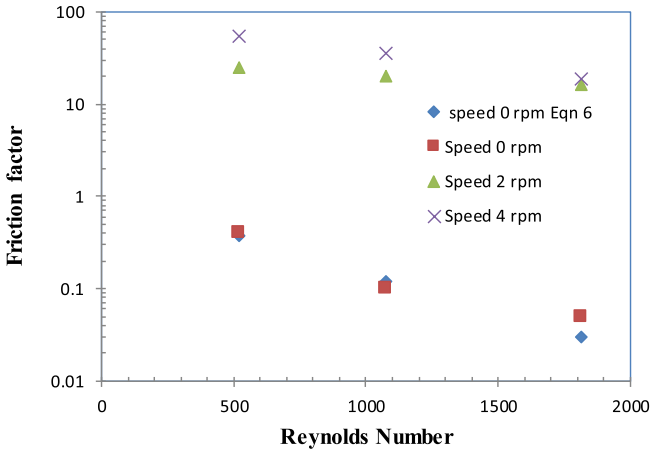

Fig. 8. Variation of friction factor for different speeds of receiver tube.

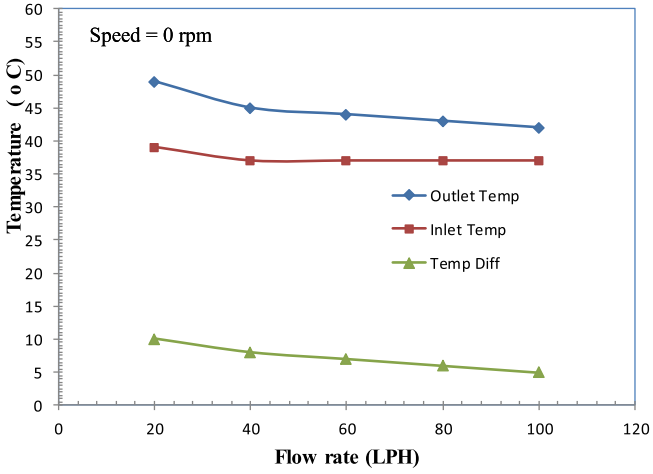

Fig. 9. Variation of outlet, inlet and temperature difference versus flow rate at a speed of 0 rpm.

lph respectively. Indeed, the fluid particles rotate several times in the tube leads to enhanced heat transfer. Fig. 11 displays the variation of working fluid temperature at a speed of 4 rpm for different mass flow rates. The results show the minimum and maximum temperature differences are 10 °C and 18 °C at 100 lph and 20 lph respectively Results

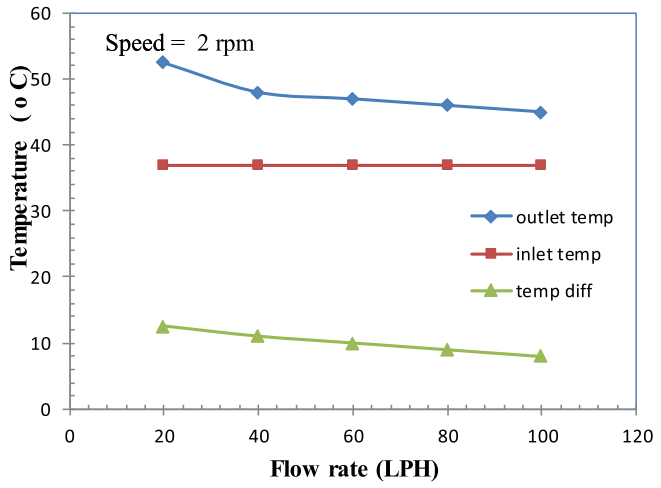

Fig. 10. Variation of outlet, inlet and temperature difference versus flow rate at a speed of 2 rpm.

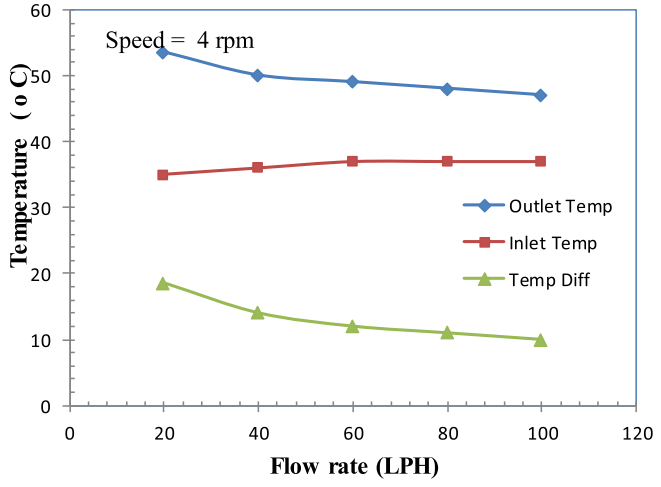

Fig. 11. Variation of outlet, inlet and temperature difference versus flow rate at a speed of 4 rpm.

also show that at low mass flow rates leads to increasing outlet temperature due to rise in available time for the exchange of heat between working fluid and wall surface. It is very clear from the results that the minimum and maximum temperature differences are not doubled when the speed of the receiver tube is changed from 2 rpm to 4 rpm. In order to study the efficiency of the collector, the collection of data was done at varied speeds of the receiver tube and mass flow rates.

Figs. 12–14 shows the enhancement of thermal efficiency at different mass flow rates and constant inlet temperature. It is clear from the figures that thermal efficiency is reduced at decreasing inlet temperature due to convection and radiation losses. In addition, by using rotary receiver tube lead to raise the thermal efficiency because of mixing of fluid particles, enhanced heat transfer coefficient and increased temperature difference. Experimental results shows that the improvement in highest thermal efficiency at a speed of 4 rpm and 2 rpm is 170% and 120% respectively in compared with stationary receiver tubes. Ultimately, the thermal efficiency for various speeds of receiver tubes at different flow rates is evaluated. The receiver tube at a speed of 4 rpm has the highest thermal efficiency of 59.23% and 50.2% and 31.4% at a speed of 2 rpm and 0 rpm respectively. The rising trend of maximum temperature difference and efficiency for different speeds of receiver are shown in Fig. 15.

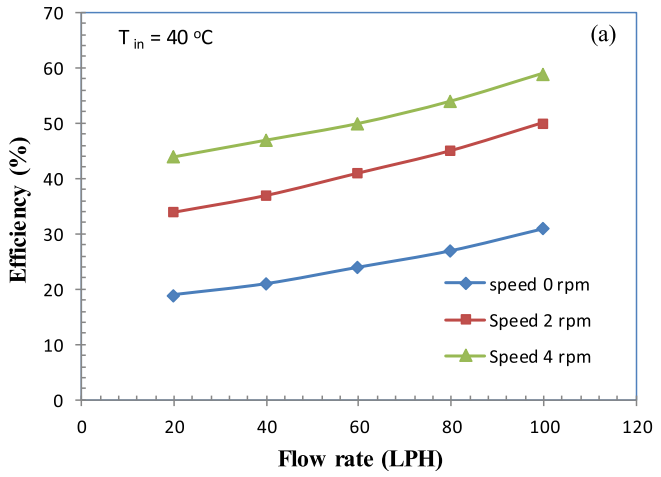

Fig. 12. Variation of efficiency with flow rate at inlet temperature of 40 °C.

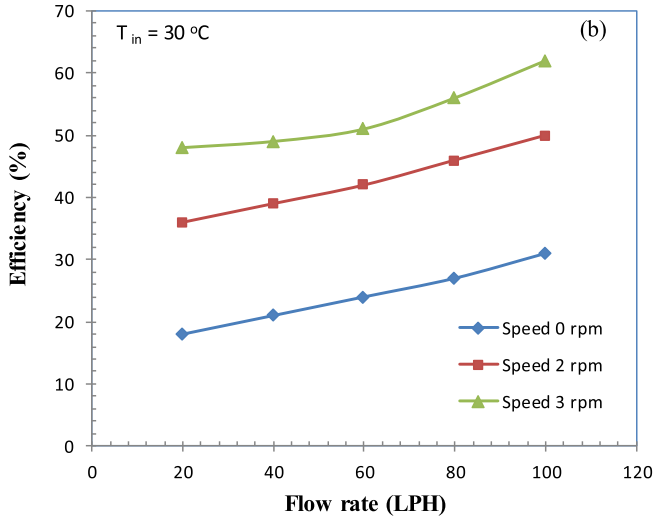

Fig. 13. Variation of efficiency with flow rate at inlet temperature of 30 °C.

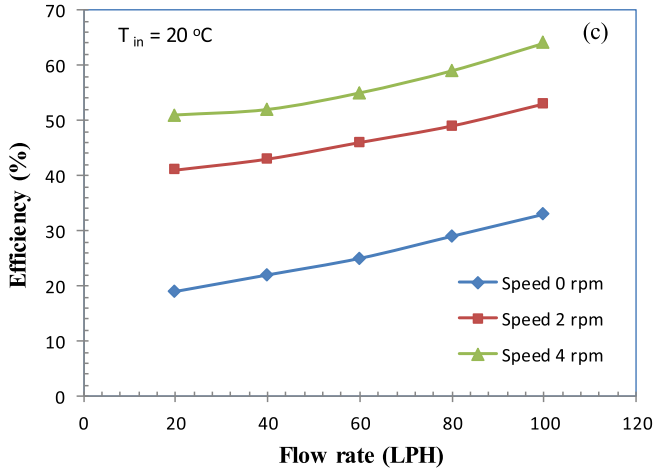

Fig. 14. Variation of efficiency with flow rate at inlet temperature of 20 °C.

Conclusions

In the present work, the enhancement of heat transfer and efficiency of a novel parabolic trough collector with rotary receiver tube was

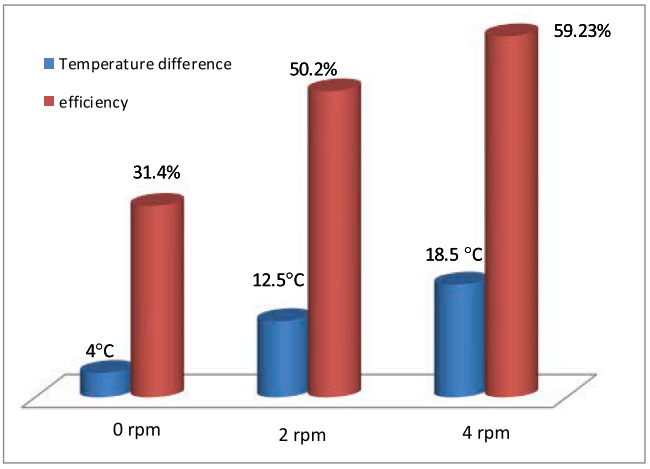

Fig. 15. Effect of different speeds of receiver tube on temperature difference and thermal efficiency.

examined experimentally. There is an increase in friction factor up to 137.5 and 62.5 times respectively for 4 rpm and 2 rpm based receiver tubes as compared to stationary tube. Rise in water temperature at a speed of 4 rpm is higher than that of 2 rpm and stationary tube. The temperature difference at a speed of 4 rpm, 2 rpm and stationary tubes are 18.5 °C, 12.5 °C and 4 °C respectively. The thermal efficiency rises by increasing the flow rate and by reducing the temperature of working fluid at inlet. Rise in thermal efficiency of the collector at a speed of 4 rpm and 2 rpm is 190.3% and 158.6% respectively as compared to that of stationary tube. Highest thermal efficiencies at a speed of 4 rpm, 2 rpm and stationary tube are found to be 59.23%, 50.2% and 31.4% respectively.

Declaration of Competing Interest

The authors declare that they have no known competing financial interests or personal relationships that could have appeared to influence the work reported in this paper.

Data availability

Data openly available in a public repository that issues datasets with DOIs. The data that support the findings of this study are openly available in, https://doi.org/10.1016/j.enconman.2014.09.056 reference number [45]. Policy: All

Acknowledgement

The authors would like to thank the Management of RajaRajeswari Group of Institutions for the financial support.

References

[1] Wang Q, Yang H, Huang X, Li J, Pei G. Numerical investigation and experimental validation of the impacts of an inner radiation shield on parabolic trough solar receivers. Appl Therm Eng 2018;132:381–92.
[2] Qiu Y, Li M-J, He Y-L, Tao W-Q. Thermal performance analysis of a parabolic trough solar collector using supercritical CO2 as heat transfer fluid under non-uniform solar flux. Appl Therm Eng 2017;115:1255–65.
[3] Loni R, Kasaeian AB, Askari Asli-Ardeh E, Ghobadian B, Le Roux WG. Performance study of a solar-assisted organic Rankine cycle using a dish-mounted rectangular-cavity tubular solar receiver. Appl Therm Eng 2016;108:1298–309.
[4] Padilla Ricardo Vasquez, Fontalvo Armando, Demirkaya Gokmen, Martinez Arnold, Quiroga Arturo Gonzalez. Exergy analysis of parabolic trough solar receiver. Appl Therm Eng 2014;67(1-2):579–86.
[5] Ghasemi SE, Ranjbar AA. Numerical thermal study on effect of porous rings on performance of solar parabolic trough collector. Appl Therm Eng 2017;118:807–16.
[6] Jin J, Ling Y, Hao Y. Similarity analysis of parabolic-trough solar collectors. Appl Energy 2017;204:958–65.
[7] Fuqiang W, Ziming C, Jianyu T, Yuan Y, Yong S, Linhua L. Progress in concentrated solar power technology with parabolic trough collector system: A comprehensive review. Renew Sustain Energy Rev 2017;79:1314–28.
[8] Muñoz J, Abánades A. Analysis of internal helically finned tubes for parabolic trough design by CFD tools. Appl Energy 2011;88:4139–49.
[9] Kasaeian A, Daneshazarian R, Mahian O, Kolsi L, Chamkha AJ, Wongwises S, et al. Nanofluid flow and heat transfer in porous media: A review of the latest developments. Int J Heat Mass Transf 2017;107:778–91.
[10] Gupta M, Singh V, Kumar R, Said Z. A review on thermophysical properties of nanofluids and heat transfer applications. Renew Sustain Energy Rev 2017;74:638–70.
[11] Hafez AZ, Attia AM, Eltwab HS, ElKousy AO, Afifi AA, AbdElhamid AG, et al. Design analysis of solar parabolic trough thermal collectors. Renew Sustain Energy Rev 2018;82(1):1215–60.
[12] Bellos E, Tzivanidis C, Antonopoulos KA, Gkinis G. Thermal enhancement of solar parabolic trough collectors by using nanofluids and converging-diverging absorber tube. Renewable Energy 2016;94:213–22.
[13] Fuqiang W, Zhexiang T, Xiangtao G, Jianyu T, Huaizhi H, Bingxi L. Heat transfer performance enhancement and thermal strain restrain of tube receiver for parabolic trough solar collector by using asymmetric outward convex corrugated tube. Energy 2016;114:275–92.
[14] Huang Z, Li Z-Y, Yu G-L, Tao W-Q. Numerical investigations on fully developed mixed turbulent convection in dimpled parabolic trough receiver tubes. Appl Therm Eng 2017;114:1287–99.
[15] Bitam EW, Demagh Y, Hachicha AA, Benmoussa H, Kabar Y. Numerical investigation of a novel sinusoidal tube receiver for parabolic trough technology. Appl Energy 2018;218:494–510.
[16] Cheng ZD, He YL, Cui FQ. Numerical study of heat transfer enhancement by unilateral longitudinal vortex generators inside parabolic trough solar receivers. Int J Heat Mass Transf 2012;55:5631–41.
[17] Xiangtao G, Fuqiang W, Haiyan W, Jianyu T, Qingzhi L, Huaizhi H. Heat transfer enhancement analysis of tube receiver for parabolic trough solar collector with pin fin arrays inserting. Sol Energy 2017;144:185–202.
[18] Benabderrahmane A, Aminallah M, Laouedj S, Benazza A, Solano JP. Heat Transfer Enhancement in a Parabolic Trough Solar Receiver using Longitudinal Fins and Nanofluids. J Therm Sci 2016;25:410–7.
[19] Reddy KS, Satyanarayana GV. Numerical study of porous finned receiver for solar parabolic trough concentrator. Eng Appl Comput Fluid Mech 2008;2(2):172–84.
[20] Muñoz J, Abánades A. A technical note on application of internally finned tubes in solar parabolic trough absorber pipes. Sol Energy 2011;85(3):609–12.
[21] Bellos E, Tzivanidis C, Tsimpoukis D. Thermal enhancement of parabolic trough collector with internally finned absorbers. Sol Energy 2017;157:514–31.
[22] Bellos E, Tzivanidis C, Tsimpoukis D. Multi-criteria evaluation of parabolic trough collector with internally finned absorbers. Appl Energy 2017;205:540–61.
[23] Bellos E, Tzivanidis C, Tsimpoukis D. Enhancing the performance of parabolic trough collectors using nanofluids and turbulators. Renew Sustain Energy Rev 2018;91:358–75.
[24] Bellos E, Tzivanidis C, Tsimpoukis D. Optimum number of internal fins in parabolic trough collectors. Appl Therm Eng 2018;137:669–77.
[25] Jaramillo OA, Borunda M, Velazquez-Lucho KM, Robles M. Parabolic trough solar collector for low enthalpy processes: An analysis of the efficiency, enhancement by using twisted tape inserts. Renewable Energy 2016;93:125–41.
[26] Mwesigye A, Bello-Ochende T, Meyer JP. Heat transfer and entropy generation in a parabolic trough receiver with wall-detached twisted tape inserts. Int J Therm Sci 2016;99:238–57.
[27] Ghadirijafarbeigloo Sh, Zamzamian AH, Yaghoubi M. 3-D numerical simulation of heat transfer and turbulent flow in a receiver tube of solar parabolic trough concentrator with louvered twisted-tape inserts. Energy Procedia 2014;49:373–80.
[28] Rawani A, Sharma SP, Singh KDP. Enhancement in performance of parabolic trough collector with serrated twisted-tape inserts. Int J Thermodyn 2017;20(2):111–9.
[29] Chang C, Xu C, Wu ZY, Li X, Zhang QQ, Wang ZF. Heat transfer enhancement and performance of solar thermal absorber tubes with circumferentially non-uniform heat flux. Energy Procedia 2015;69:320–7.
[30] Zhu X, Zhu L, Zhao J. Wavy-tape insert designed for managing highly concentrated solar energy on absorber tube of parabolic trough receiver. Energy 2017;141:1146–55.
[31] Song X, Dong G, Gao F, Diao X, Zheng L, Zhou F. A numerical study of parabolic trough receiver with nonuniform heat flux and helical screw-tape inserts. Energy 2014;77:771–82.
[32] Liu Y, Chen Q, Hu K, Hao J-H. Flow field optimization for the solar parabolic trough receivers in direct steam generation systems by the variational principle. Int J Heat Mass Transf 2016;102:1073–81.
[33] Diwan K, Soni MS. Heat transfer enhancement in absorber tube of parabolic trough concentrators using wire-coils inserts. Univ J Mech Eng 2015;3(3):107–12.
[34] Şahin HM, Baysal E, Rıza Dal A, Şahin N. Investigation of heat transfer enhancement in a new type heat exchanger using solar parabolic trough systems. Int J Hydrogen Energy 2015;40(44):15254–66.
[35] Jamal-Abad MT, Saedodin S, Aminy M. Experimental investigation on a solar parabolic trough collector for absorber tube filled with porous media. Renewable Energy 2017;107:156–63.
[36] Wang P, Liu DY, Xu C. Numerical study of heat transfer enhancement in the receiver tube of direct steam generation with parabolic trough by inserting metal foams. Appl Energy 2013;102:449–60.

[37] Mwesigye A, Bello-Ochende T, Meyer JP. Heat transfer and thermodynamic performance of a parabolic trough receiver with centrally placed perforated plate inserts. Appl Energy 2014;136:989–1003.
[38] Mwesigye A, Bello-Ochende T, Meyer JP. Multi-objective and thermodynamic optimisation of a parabolic trough receiver with perforated plate inserts. Appl Therm Eng 2015;77:42–56.
[39] Chang C, Sciacovelli A, Wu Z, Li X, Li Y, Zhao M, et al. Enhanced heat transfer in a parabolic trough solar receiver by inserting rods and using molten salt as heat transfer fluid. Appl Energy 2018;220:337–50.
[40] Bellos E, Tzivanidis C. Investigation of a star flow insert in a parabolic trough solar collector. Appl Energy 2018;224:86–102.
[41] Kumar KR, Reddy KS. Thermal analysis of solar parabolic trough with porous disc receiver. Appl Energy 2009;86:1804–12.
[42] Reddy KS, Ravi Kumar K, Ajay CS. Experimental investigation of porous disc enhanced receiver for solar parabolic trough collector. Renewable Energy 2015;77:308–19.
[43] Zheng Z, Xu Y, He Y-L. Thermal analysis of a solar parabolic trough receiver tube with porous insert optimized by coupling genetic algorithm and CFD. Sci China Tech Sci 2016;59:1475–85.
[44] Too YCS, Benito R. Enhancing heat transfer in air tubular absorbers for concentrated solar thermal applications. Appl Therm Eng 2013;50(1):1076–83.
[45] Biencinto M, A new concept of solar thermal power plants with large-aperture parabolic-trough collectors and sCO2 as working fluid, Energy Convers Manage 2019;1:1.112030.
[46] Kumar Anil, Vyas Savita, Nchelatebe Nkwetta Dan. Experimental study of single slope solar still coupled with parabolic trough collector. Mater Sci Energy Technol 2020;3:700–8.
[47] Wu Shaobing, Tang Runsheng, Wang Changmei. Numerical calculation of the intercept factor for parabolic trough solar collector with secondary mirror. Energy 2021;233:121175.
[48] Kasaeian Alibakhsh, Daviran Samaneh, Azarian Reza Danesh, Rashidi Alimorad. Performance evaluation and nanofluid using capability study of a solar parabolic trough collector. Energy Convers Manag 2015;89:368–75.
[49] A. Standard, Standard 93-2010. Method of testing to determine the thermal performance of solar collectors, American Society for Heating, Refrigerating and Air-conditioning Engineers, Atlanta, USA, 2010.
[50] Valizade M, Heyhat MM. Experimental study of the thermal behavior of direct absorption parabolic trough collector by applying copper metal foam as volumetric solar absorption. Renew Energy 2020;145:261–9.

Study on Heat transfer and Pressure Drop in Tube-In-Tube Helical Heat Exchanger

N Sreenivasalu Reddy[1,*], Vishwanath K C[1], Satheesha V[1], Thejaraju R[2], Karthik Raj N[1], Manoj M [1], Goutham H[1], and Manjunatha B S[1]

[1] *Department of Mechanical Engineering, Rajarajeswari College of Engineering, Bangalore, 560074, India Affiliated to Visvesvaraya Technological University, Belagavi, Karnataka, India*
[2] *Department of Mechanical and Automobile Engineering, CHRIST Deemed to be University, Bangalore, 560074, India*
[*] *Corresponding author. E-mail: nsreddysrsit@gmail.com*

Received: Aug. 10, 2020, Accepted: Mar. 23, 2021

The present work aims to investigate the effect of different configurations of the tube-in-tube helically coiled heat exchanger. Commercial CFD codes were used to predict the fluid flow and heat transfer in a tube-in-tube helical heat exchanger. The model of different configurations of the inner tube has been simulated by varying the Dean number. The numerical results are verified and found to be in good agreement with reported data in the literature. Nusselt Number and friction factor are evaluated for different angular positions. The use of geometry E increases the Nusselt number and friction factor by 19.05% and 16% respectively at a Dean number of 4000 as compared with a circular tube as compared with the circular tube.

KEYWORDS: Heat exchanger; Dean number; Nusselt number; Friction factor

http://dx.doi.org/10.6180/jase.202108_24(4).0019

1. Introduction

Tube-in-tube (TIT) helically coiled heat exchangers are compact in design and high thermal stress adaptability plays a major role in a cold storage system, air cooling system, heat transfer applications, thermal power plants, food-based industries, chemical factories, and desalination of water [1–3]. Helically shaped coiled pipe posses a high heat transfer coefficient, higher resistance of flow, and higher efficiency due to rotary motion. Also activates the fluid to flow along the external surface of the rotary tube. It assists in raising the pressure on the outer surface than the inner surface of the helically shaped coiled tube heat exchanger [4–12].

As compared with a straight-coiled pipe, the characteristics of fluid flow in a helically shaped coiled tube is complex in nature. Rogers et al. [13] studied the heat transfer and friction factor of fluid passing through the helically shaped coiled pipe, for a range of Reynolds Number (10,000 -100,000). Liu et al. [14] studied two-phase flow analysis experimentally using a helically shaped coiled tube. Murai et al. [15] investigated heat transfer and fluid flow using CFD (Computational Fluid Dynamics) and given more opportunities to study the behaviour of the flow in TIT helically coiled heat exchangers.

Jayakumar et al. [16] proved that the flow in two-phase can achieve the hydraulic properties of the helically shaped tube. Pan et al. [17] explained the improvements in heat transfer along with the passive technique in the helical tube. Sharifi et al. [18] proved that the improvement in Nusselt Number and thermal properties of helically coiled heat exchanger using wire coil inserts. Ju-Lee et al. [19] studied the characteristics of a fluid flow of the spirally shaped pipe. Kumar et al. [20] investigated the effects of the transfer of heat and causes of hydrodynamics in TIT helically shaped coiled pipe heat exchanger.

M. A. Omara et al. [21] studied the heat transfer and

friction factor using a twisted elliptical tube with a helical coil. S. K. Naghibzadeh et al. [22] investigated the heat transfer experimentally by using a helical coil tube with a flattened cross-section. S. W. Chang et al. [23] studied the heat transfer and friction factor numerically using a helical coil with a twisted section.

The present work aims to study the performance of TIT helically shaped coiled pipe heat exchanger with different geometries of the inner tube. This is the first investigation on such types of heat exchangers, which have not been studied previously.. The Nusselt Numer of the TIT helically shaped coiled pipe heat exchanger with different geometries of the inner tube is compared with the tube in tube circular helical heat exchanger.

From the available literature survey it can be clearly understood that tube-in-tube helically coiled heat exchanger has drawn very much concentration of research and the computational fluid dynamics (CFD) analysis is a useful analytical tool for carrying out heat transfer and pressure drop studies and can be extended for wide range of process conditions with much ease.

Further, literature survey indicates the heat transfer can be enhanced by modifying the geometry and different shaped tubes. However, it appears that lesser published information is available on systematic study of flow and heat transfer tube-in-tube helically coiled heat exchanger. Therefore, in the present investigation, it has been proposed to systematically carryout studies on flow and heat transfer tube-in-tube helically coiled heat exchanger. This may be useful for handling practical engineering applications.

Also, the present paper presents the CFD (Computational Fluid Dynamics) results to specify the increase in heat transfer rate with passive technique in the TIT helically shaped coiled pipe heat exchanger. Numerical tests were conducted by varying Dean number.

2. Modeling

Computational Fluid Dynamics (CFD) is a process of solving fluid flow analysis and heat transfer using numerical methods. In this investigation CFD Model is used to analyses the flow simulation inside the tube-in-tube helically coiled heat exchanger for various geometry configurations and studied the Nusselt number distribution over the surface at various Dean number. Modelling is built for proposed research work and simulation is also carried out for the process of using a model to study the behaviour and performance of a theoretical system. Figure 1 shows the vertically placed helically shaped coiled tube heat exchanger with its specification. Figure 2 shows mesh details. Curvature $\delta = d/\mathbf{R_c}$ is defined as the ratio of tube diameter to the coil diameter and $\lambda = H/\pi\mathbf{R_c}$ is defined as the ratio of pitch to the developed length of a single turn. Dean Number is termed as $De = Re\delta^{0.5}$, where Re is the Reynolds Number

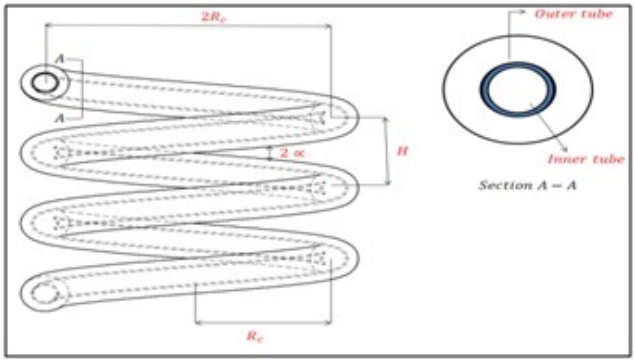

Fig. 1. Geometry of a helical pipe.

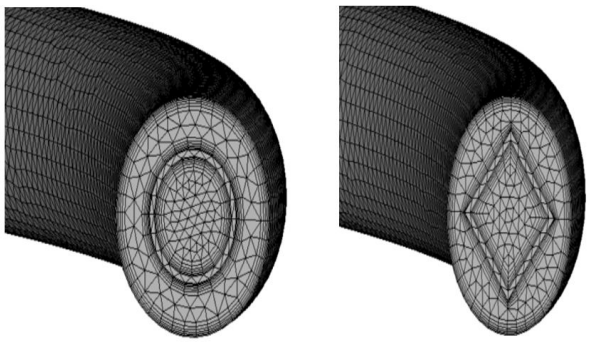

Fig. 2. Polyhedral mesh for different modified shaped tubes

TIT helically coiled tube heat exchanger consists of two helically shaped tubes, which are concentric in nature. Cold fluid flows in the annulus and the hot fluid flows in the inner tube. The simulation geometry was generated in ANSYS Workbench 18.1 and meshes were generated in Altair Hyper Mesh 13.0. To perform the CFD analysis, mesh grids are generated on the helically shaped tube and which are created using polyhedral mesh. The mesh density was made to improve from 0.038617 cells m^{-3} to $8{\times}10^6$ cells m^{-3}. The SIMPLE scheme has been used for Pressure-velocity coupling. The momentum equation has been detached by the

QUICK scheme. Turbulent kinetic energy was coupled using the QUICK scheme. The accuracy level for the simulation is maintained by the value of 1.0 e^{-04} in continuity, velocities, k, and ϵ. The energy equation was detached by the QUICK scheme. The post-processing is carried out using CFD-Post 18.1 which provides the contours of different configurations regarding the thermal parameters, animation, and angular positions of the helical tube. Table 1 and 2 shows the geometry details.

Simulations were carried out at different Dean numbers of 2000, 2250, 2500, 3000, 3500, and 4000 for an annulus keeping the constant design. The inlet and outlet temperatures in the internal tube were fixed at 300 K and 380 K, respectively. The direction of hot and cold fluid is considered as counter flow in the present simulation. The reason for a fixed temperature at the inlet of the tube is to avoid two-phase flow.

Table 1. Geometry with different shaped tubes.

Parameters	Inner Tube	Outer Tube
External diameter (m)	0.026	0.0508
Helical diameter (m)	0.77	0.77
Pitch (m)	0.1	0.1
Velocity (m/s)	0.073	0.3-0.8
Dean number (dimensionless)	1000	1930-4140
Prandtl number (dimensionless)	7	7

Table 2. Geometry and its Dimensions

Geometry	Design Modification
A	Circular Tube
B	Square Tube
C	Ellipse Tube
D	Pentagon Tube
E	Hexagon Tube

The mesh selection for all geometries is in the range of 17.5×10^6 and 24×10^6, with the intension of error lesser than 1%. Mesh independence study was carried out and as shown in figure 3, for individual geometries using a various number of elements and Nusselt Number. The mesh elements do not cause any error to the results when the elements numbers are greater than 20×10^6 from geometry B to E. The selection of temperature at the inlet of the inner tube and outer tube is 300K and 380K respectively. The constant velocity is applied at the inlet to the inner tube. Computations were carried by varying the Dean Number from 2000 – 4000 respectively. The computations were setup at convergence criterion of continuity up to 10^{-4} . The number of iterations was carried out up to 1000. The Dean number is calculated using equation 1

$$\mathrm{De} = \frac{\rho \mathrm{v} \mathrm{D_h}}{\mu}\sqrt{\delta} \tag{1}$$

Where ρ represents density, v represents velocity in m/s, μ is the dynamic viscosity, and D_h is the hydraulic diameter.

$$D_h = \frac{4A}{P} \tag{2}$$

Where P is the perimeter of the coil and A is the cross-sectional area Curvature ratio, λ

$$\lambda = \frac{d_o}{D_c} \tag{3}$$

Where d_o and D_c are the outer diameter of the inner tube and helical diameter respectively. Differential equations that govern turbulent flow have been written in the vector form as shown in equation 4. Continuity equation

$$\frac{\partial \rho \mathrm{u_i}}{\partial \mathrm{x_i}} = 0 \tag{4}$$

Momentum equation

$$\frac{\partial\left(\rho \mathrm{u_i u_j}\right)}{\partial \mathrm{x_j}} + \frac{\partial \mathrm{P}}{\partial \mathrm{x_i}} - \frac{\partial}{\partial \mathrm{x_j}}\left[(\mu+\mu_t)\left(\frac{\partial \mathrm{u_i}}{\partial \mathrm{x_j}} + \frac{\partial \mathrm{u_j}}{\partial \mathrm{x_i}}\right)\right] - \mathrm{F_i} = 0 \tag{5}$$

Energy equation

$$\frac{\partial\left(\rho E_{\mathrm{uj}}\right)}{\partial \mathrm{x_j}} + \frac{\partial\left(\mathrm{Pu_j}\right)}{\partial \mathrm{x_j}} - \varnothing - \frac{\partial}{\partial \mathrm{x_j}} \mathrm{k}\left(\frac{\partial \mathrm{T}}{\partial \mathrm{x_j}}\right) = 0 \tag{6}$$

Where $\varnothing$ is the viscous heating, it is shown in equation 7.

$$\varnothing = \mu \frac{\partial \mathrm{u_i}}{\partial \mathrm{x_j}}\left(\frac{\partial \mathrm{u_i}}{\partial \mathrm{x_j}} + \frac{\partial \mathrm{u_j}}{\partial \mathrm{x_i}}\right) \tag{7}$$

Turbulent kinetic energy is given by equation 8

$$\frac{\partial\left(\rho \mathrm{u_j k}\right)}{\partial \mathrm{x_j}} - \frac{\partial}{\partial \mathrm{x_j}}\left[\left(\mu + \frac{\mu_t}{\sigma_k}\right)\frac{\partial \mathrm{k}}{\partial \mathrm{x_j}}\right] - \mathrm{P_k} + \rho\varepsilon = 0 \tag{8}$$

where k denotes the kinetic energy subjected to turbulence.

σ_k is the turbulent Prandtl Number. Pkis the turbulent kinetic energy shown in the equation 9

$$P_{\mathrm{k}} = \mu_t\left(\frac{\partial \mathrm{u_i}}{\partial \mathrm{x_j}} + \frac{\partial \mathrm{u_j}}{\partial \mathrm{x_j}}\right)\frac{\partial \mathrm{u_i}}{\partial \mathrm{x_j}} \tag{9}$$

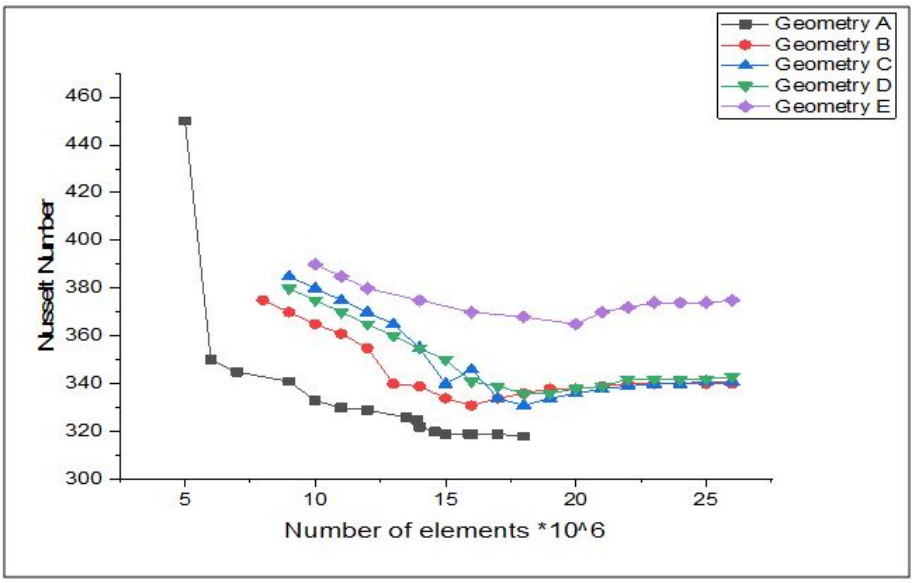

Fig. 3. Mesh independence study.

Where ε represents dissipation of kinetic energy is given by the equation 10

$$\frac{\partial\left(\rho u_j \varepsilon\right)}{\partial x_j} - \frac{\partial}{\partial x_j}\left[\left(\mu - \frac{\mu_t}{\sigma_\varepsilon}\right)\frac{\partial \varepsilon}{\partial x_j}\right] - \frac{\varepsilon}{k}\left(C_{\varepsilon 1} P_k - C_{\varepsilon 2}\rho\varepsilon\right) = 0 \tag{10}$$

The k-ε model is given by equation 11

$$\mu_t = C_\mu \rho \frac{k^2}{\varepsilon} \tag{11}$$

Where ρ indicates density and C_μ is constant. $C_{\varepsilon 1} = 1.47, C_{\varepsilon 2} = 1.92, \sigma_k = 1.0 \sigma_\varepsilon = 1.3$, and $C_\mu = 0.09$ The values of these constants are the same as those of Launder and Spalding [15], the ideas of [13] for $C_{\varepsilon 1}$ are used in this analysis.

3. Results and discussion

The present simulated model results are verified with the results of [20]. Figure 4 shows the variation of Nusselt number versus Dean number for Geometry A. The results show that the numerical results of geometry A and experimental data reported by [20] tend to be the same. An average Nusselt Number ΔNu has been calculated as per the equation 12

$$\Delta Nu = \frac{\sum_1^5 \left[100 - \frac{Nu_i * 100}{Nu_A}\right]}{5} \tag{12}$$

Where Nu_i indicates the Nusselt Number for modified geometries. Nu_A is the Nusselt Number of Geometry A. Figure 5 shows the variation of Nu with Dean number, and it is evident from the figure that ΔNu of Geometry B increases approximately 14.73% as compared to Geometry A. It is observed that the increase of ΔNu from Geometry B to C in the inner tube is 1.5% and geometry C to E is 3.1

Figure 5 shows the relationship between the Nusselt number and the Dean number for different geometries. It is clear from figure 6 that there is a rise in Nussel number as the Dean number increases. Figure 7 represents the velocity contours for the inner tube of five different geometries of the TIT helically coiled heat exchanger. Rows represent the different geometry of the TIT helically coiled heat exchanger. The columns show different cross-sections (0^o, 30^o, 90^o, 180^o, 270^o, and 360^o). It is observed from the figure that the modified geometries i.e. from B to E, the contours of velocity changes at 30^o position and recognizing different profiles of velocity. However, from 90^o to 360^o slight changes in the profile (patterns) have been observed. The pattern of velocity is proof of the total development of the fluid flow. For the geometries, A, B, C, D, and E, the maximum value of velocity is observed towards the surface of the outside tube.

Figure 8 represents the contours of the temperatures in the inner pipe for the different configurations of TIT helically coiled heat exchanger. The maximum values of temperature are observed towards the outside of the tube, due to the generation of the vortex. Figure 8 also signifies an increase in

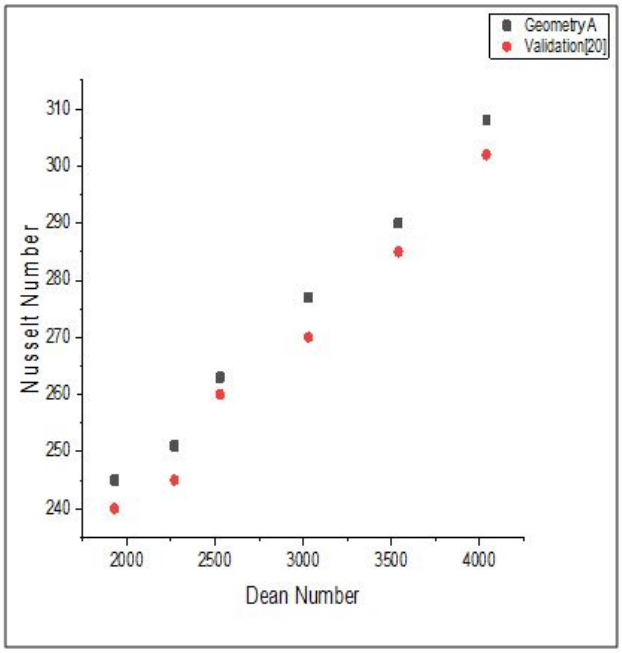

Fig. 4. Nusselt number versus Dean number.

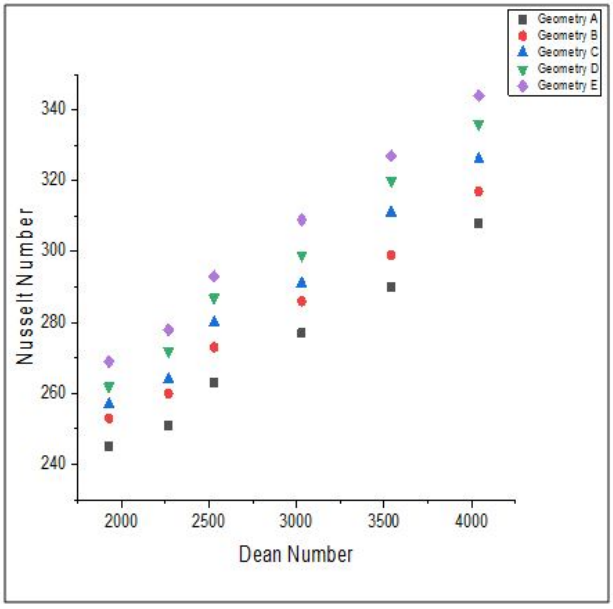

Fig. 5. Nusselt number versus Dean Number.

the patterns for the angular positions 30° to 360° due to more surface area. Figure 9 represents the velocity contours in the annulus. For the geometries from (B) to (E), it is enough to confirm that there is a developed fluid flow in the annulus.

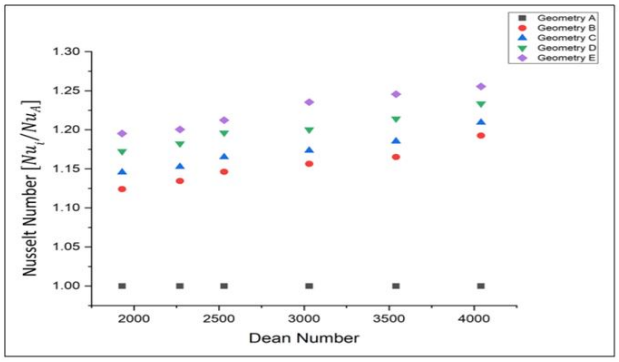

Fig. 6. Nusselt number versus Dean Number.

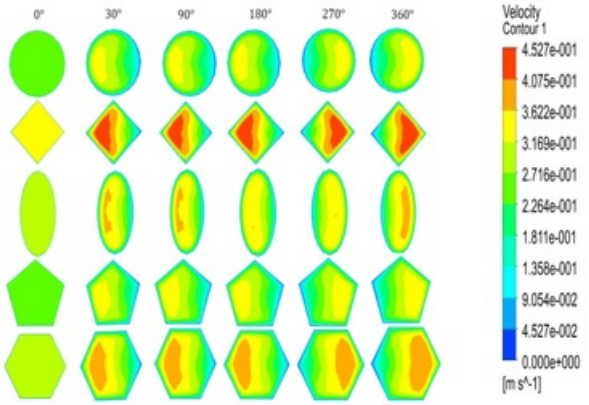

Fig. 7. Velocity contours of the inner tube.

It is also observed from the velocity contours that, the secondary flow from geometry (B) to (E) has greater turbulence than geometry (A). Figure 11 illustrates the temperature contours in the annulus. It is noticed that there is a significant rise in temperature in the annulus at an angular position of 360°. For models from B to E, the temperature amplified uniformly and there are no significant temperature differences among the models. Figure 5 to 10 provides the proof of an increase in Nusselt Number subjected to Dean Number. The increase of heat transfer from geometry A to E is due to the passive technique, better surface area, and centrifugal force.

Figure 11 shows the prediction of the numerical results of the Darcy-Weisbach friction factor with Dean Number. It is observed in figure 11 that there is a decrease in the frictional factor as the Dean number decreases. When compared to Geometry B to C, the frictional factor is increased by 8.54%. The decrease in frictional factor indicates that there is a decrease

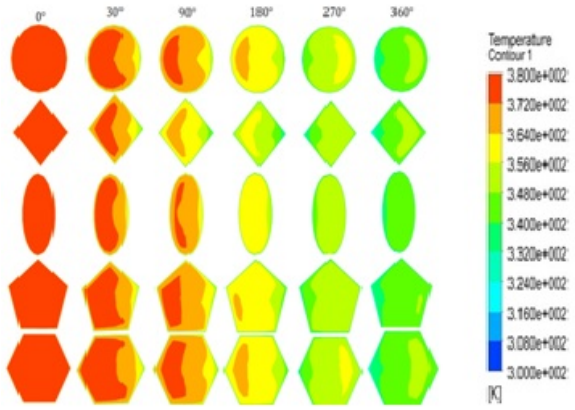

Fig. 8. Temperature contours of internal pipe.

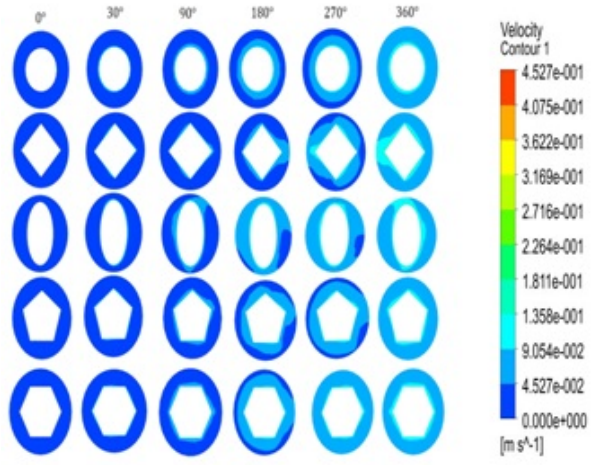

Fig. 9. Velocity contours for the outer pipe.

in pressure drop since both are directly proportional. This depletion is due to the cross-sectional area of the geometry which is bigger than the circular tube. As the surface area is better enough (Geometry D and E) friction factor gradually increases by 4%. In the case of Geometry C to D, the friction factor is increased by 7%.

4. Conclusions

- The use of geometry E increases the Nusselt number and friction factor by 128 19.05% and 16% respectively as compared with the circular tube. ΔNu of Geometry B increases by 14.73% as compared to Geometry A. It is observed that the increase of ΔNu from Geometry B to C in the inner tube is 1.5% and geometry C to E is 3.1%.

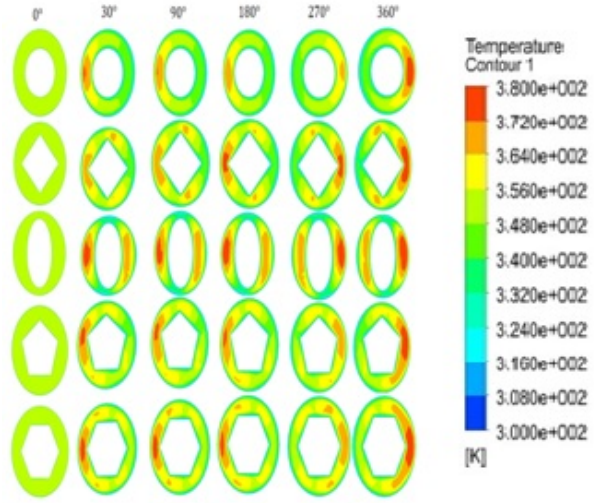

Fig. 10. Temperature contours in the annulus.

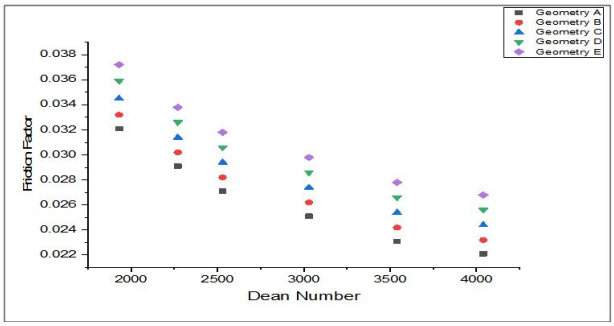

Fig. 11. Friction factor verses Dean Number .

- The use of geometry E increases the Nusselt number and friction factor by 128 19.05% and 16% respectively as compared with the circular tube. ΔNu of Geometry B increases by 14.73% as compared to Geometry A. It is observed that the increase of ΔNu from Geometry B to C in the inner tube is 1.5% and geometry C to E is 3.1%.

- When compared to Geometry B to C, the frictional factor is increased by 8.54%. The decrease in frictional factor indicates that there is a decrease in pressure drop since both are directly proportional. This depletion is due to the more cross-sectional area of the geometry than the circular tube. As the surface area is better enough (Geometry D and E) friction factor gradually increases

by 4%. In the case of Geometry C to D, the friction factor is increased by 7%.

- For the geometries from B to E, it is enough to confirm that there is a developed fluid flow in the annulus region. It is also observed from the velocity contours that, the secondary flow from geometry B to E has greater turbulence than geometry A.

Acknowledgments

The authors would like to gratefully acknowledge the support of the management of Rajarajeswari group of institutions (RRGI) for this original research work.

References

[1] Michele Ciofalo, Antonino Arini, and Massimiliano Di Liberto. On the influence of gravitational and centrifugal buoyancy on laminar flow and heat transfer in curved pipes and coils. *International Journal of Heat and Mass Transfer*, 82:123–134, 2015. ISSN 00179310.

[2] Hamid Saffari, Rouhollah Moosavi, Nourooz Mohammad Nouri, and Cheng Xian Lin. Prediction of hydrodynamic entrance length for single and two-phase flow in helical coils. *Chemical Engineering and Processing: Process Intensification*, 86:9–21, oct 2014. ISSN 02552701.

[3] M. R.H. Nobari, B. Shiniyan, and M. Mirzaei. Mixed convection in a vertical helical annular pipe. *International Journal of Heat and Mass Transfer*, 73:468–482, 2014. ISSN 00179310.

[4] Liejin Guo, Ziping Feng, and Xuejun Chen. An experimental investigation of the frictional pressure drop of steam-water two-phase flow in helical coils. *International Journal of Heat and Mass Transfer*, 44(14):2601–2610, 2001. ISSN 00179310.

[5] Liang Zhao, Liejin Guo, Bofeng Bai, Yucheng Hou, and Ximin Zhang. Forced convective boiling heat transfer and pressure drop characteristics of two-phase flow inside a small horizontal helically coiled tubing once-through steam generator. In *Proceedings of the ASME Summer Heat Transfer Conference*, volume 2003, pages 677–685, 2003. ISBN 0791836940.

[6] Huaiming Ju, Zhiyong Huang, Yuanhui Xu, Bing Duan, and Yu Yu. Hydraulic performance of small bending radius helical coil-pipe. *Journal of Nuclear Science and Technology*, 38(10):826–831, 2001. ISSN 00223131.

[7] R. C. Xin, A Awwad, Z. F. Dong, M. A. Ebadian, and H. M. Soliman. An investigation and comparative study of the pressure drop in air-water two-phase flow in vertical helicoidal pipes. *International Journal of Heat and Mass Transfer*, 39(4):735–743, 1996. ISSN 00179310.

[8] R. C. Xin, A. Awwad, Z. F. Dong, and M. A. Ebadian. An experimental study of single-phase and two-phase flow pressure drop in annular helicoidal pipes. *International Journal of Heat and Fluid Flow*, 18(5):482–488, 1997. ISSN 0142727X.

[9] A. Awwad, R. C. Xin, Z. F. Dong, M. A. Ebadian, and H. M. Soliman. Measurement and correlation of the pressure drop in air-water two-phase flow in horizontal helicoidal pipes. *International Journal of Multiphase Flow*, 21(4):607–619, 1995. ISSN 03019322.

[10] A. B. Biswas and S. K. Das. Two-phase frictional pressure drop of gas-non-Newtonian liquid flow through helical coils in vertical orientation. *Chemical Engineering and Processing: Process Intensification*, 47(5):816–826, may 2008. ISSN 02552701.

[11] Lorenzo Santini, Andrea Cioncolini, Carlo Lombardi, and Marco Ricotti. Two-phase pressure drops in a helically coiled steam generator. *International Journal of Heat and Mass Transfer*, 51(19-20):4926–4939, sep 2008. ISSN 00179310.

[12] Marco Colombo, Luigi P.M. Colombo, Antonio Cammi, and Marco E. Ricotti. A scheme of correlation for frictional pressure drop in steam-water two-phase flow in helicoidal tubes. *Chemical Engineering Science*, 123:460–473, feb 2015. ISSN 00092509.

[13] G. F.C. Rogers and Y. R. Mayhew. Heat transfer and pressure loss in helically coiled tubes with turbulent flow. *International Journal of Heat and Mass Transfer*, 7(11):1207–1216, 1964. ISSN 00179310.

[14] X. F. Liu, G. D. Xia, and G. Yang. Experimental study on the characteristics of air-water two-phase flow in vertical helical rectangular channel. *International Journal of Multiphase Flow*, 73:227–237, jul 2015. ISSN 03019322.

[15] Yuichi Murai, Shinji Yoshikawa, Shin Ichi Toda, Masa Aki Ishikawa, and Fujio Yamamoto. Structure of air-water two-phase flow in helically coiled tubes. *Nuclear Engineering and Design*, 236(1):94–106, jan 2006. ISSN 00295493.

[16] J S Jayakumar, S M Mahajani, J C Mandal, P K Vijayan, and Rohidas Bhoi. Experimental and CFD estimation of heat transfer in helically coiled heat exchangers. *Chemical*

Engineering Research and Design, 86(3):221–232, 2008. ISSN 02638762.

[17] Changzhao Pan, Yuan Zhou, and Junjie Wang. CFD study of heat transfer for oscillating flow in helically coiled tube heat-exchanger. *Computers and Chemical Engineering*, 69:59–65, oct 2014. ISSN 00981354.

[18] Khashayar Sharifi, Morteza Sabeti, Mehdi Rafiei, Amir H. Mohammadi, and Laleh Shirazi. Computational fluid dynamics (CFD) technique to study the effects of helical wire inserts on heat transfer and pressure drop in a double pipe heat exchanger. *Applied Thermal Engineering*, 128:898–910, 2018. ISSN 13594311.

[19] Hyung Ju Lee, Jaiyoung Ryu, and Seong Hyuk Lee. Influence of perforated fin on flow characteristics and thermal performance in spiral finned-tube heat exchanger. *Energies*, 12(3), feb 2019. ISSN 19961073.

[20] Vimal Kumar, Supreet Saini, Manish Sharma, and K. D.P. Nigam. Pressure drop and heat transfer study in tube-in-tube helical heat exchanger. *Chemical Engineering Science*, 61(13):4403–4416, jul 2006. ISSN 00092509.

[21] M. A. Omara and Mohamed A. Abdelatief. Experimental study of heat transfer and friction factor inside elliptic tube fixed with helical coils. *Applied Thermal Engineering*, 134:407–418, apr 2018. ISSN 13594311.

[22] S. K. Naghibzadeh, M. R. Hajmohammadi, and M. Saffar-Avval. Heat transfer enhancement of a nanofluid in a helical coil with flattened cross-section. *Chemical Engineering Research and Design*, 146:36–47, jun 2019. ISSN 02638762.

[23] S. W. Chang, P. S. Wu, W. L. Cai, and J. H. Liu. Turbulent flow and heat transfer of helical coils with twisted section. *Applied Thermal Engineering*, 180, nov 2020. ISSN 13594311.

Materials Today: Proceedings xxx (xxxx) xxx

Contents lists available at ScienceDirect

Materials Today: Proceedings

journal homepage: www.elsevier.com/locate/matpr

Analysis of tube-in-tube copper helical heat exchanger to improve heat transfer

N. Sreenivasalu Reddy [a,*], S. Gowreesh Subramanya [b], K.C. Vishwanath [a], S. Kanchiraya [c], V. Satheesha [a], M. Karthikeyan [a]

[a] Rajarajeswari College of Engineering, Department of Mechanical Engineering, Visvesvaraya Technological University, Bengaluru 560074, India
[b] JSS Academy of Technical Education, Department of Mechanical Engineering, Visvesvaraya Technological University, Bengaluru 560060, India
[c] Government Engineering College, Department of Mechanical Engineering, Visvesvaraya Technological University, Hasan 573202, India

ARTICLE INFO

Article history:
Received 22 September 2020
Received in revised form 26 October 2020
Accepted 3 November 2020
Available online xxxx

Keywords:
Heat exchanger
Dean Number
Nusselt Number
Friction factor

ABSTRACT

The present work aims to investigate the effect of different configurations of tube-in-tube helically coiled heat exchanger. Commercial CFD codes were used to predict the fluid flow and heat transfer in a tube-in-tube helical heat exchanger. The model of different configurations of the inner tube has been simulated by varying the dean number. The numerical results are verified and found to be in good agreement with reported data in the literature. Nusselt Number and friction factor are evaluated for different angular positions. The use of geometry E increases the Nusselt Number and friction factor by 17.05% and 15% respectively at a Dean number of 400 as compared with a circular tube.

1. Introduction

Tube-in-tube (TIT) helically coiled heat exchangers are compact in design and high thermal stress adaptability plays a major role in the cold storage system, air-cooling system, heat transfer applications, thermal power plants, food-based industries, chemical factories, and desalination of water [1–3]. Helically shaped coiled pipe possess a high heat transfer coefficient, higher resistance of flow, and higher efficiency due to rotary motion. Also activates the fluid to flow along the external surface of the rotary tube. It assists in raising the pressure on the outer surface than the inner surface of the helically shaped coiled tube heat exchanger [4–6]. R.C. Xin et al. [7] investigated heat transfer and pressure drop of multi-phase flow and single-phase flow using helicoidal pipes. R.C. Xin et al. [8] compared the pressure drop in air–water two-phase flow using vertical helicoidal pipes. A. Awwad et al. [9] made a correlation of frictional factor for two-phase flow using the helical coil. A. B. Biswas et al. [10] studied pressure drop of non-Newtonian liquid flow in a vertical oriented helical coil. L. Santini et al. [11] investigated heat transfer experimentally in a helically coiled evaporator. M. Colombo et al. [12] studied heat transfer and pressure drop numerically and made a correlation of pressure drop in a two-phase flow using helicoidal tubes.

As compared with a straight-coiled pipe, the characteristics of fluid flow in a helically shaped coiled tube are complex in nature. Rogers et al. [13] studied the heat transfer and friction factor of fluid passing through the helically shaped coiled pipe, for a range of Reynolds Number (10,000–100,000). Liu et al. [14] studied two-phase flow analysis experimentally using a helically shaped coiled tube. Murai et al. [15] investigated heat transfer and fluid flow using CFD (Computational Fluid Dynamics) and given more opportunities to study about the behavior of the flow in TIT helically coiled heat exchangers.

Jayakumar et al. [16] proved that the flow in two-phase can achieve the hydraulic properties of a helically shaped tube. Pan et al. [17] explained about the improvements of heat transfer along with the passive technique in the helical tube. Sharifi et al. [18] proved that the improvement in Nusselt Number and thermal properties of helically coiled heat exchanger using wire coil inserts. Ju-Lee et al. [19] studied the characteristics of a fluid flow of a spirally shaped pipe.

Kumar et al. [20] investigated the effects of heat transfer and the causes of hydrodynamics in TIT helically shaped coiled pipe

* Corresponding author.
E-mail address: nsreddysrsit@gmail.com (N. Sreenivasalu Reddy).

https://doi.org/10.1016/j.matpr.2020.11.043
2214-7853/

heat exchanger and discussed the CFD results to specify the increase in heat transfer rate with passive technique in the TIT helically shaped coiled pipe heat exchanger. M. A. Omara et al. [21] studied the heat transfer and friction factor using a twisted elliptical tube with a helical coil. S. K. Naghibzadeh et al. [22] investigated the heat transfer experimentally by using a helical coil tube with a flattened cross-section. S. W. Chang et al. [23] studied the heat transfer and friction factor numerically using a helical coil with a twisted section.

In the present work, an attempt is made to study characteristics of the fluid flow and heat transfer for different geometries of TIT helically shaped heat exchanger in the laminar zone. Different geometries of the internal tube of TIT helically shaped heat exchanger are made by keeping surface area is constant. Numerical tests were conducted by varying Dean Number.

2. Modeling

Fig. 1 shows the vertically placed helically shaped coil tube heat exchanger with its specification. Curvature $\delta = d/R_c$ is defined as the ratio of tube diameter to the coil diameter and $\lambda = H/\pi R_c$ is defined as the ratio of pitch to the developed length of a single turn. Dean Number is termed as $De = Re\ \delta^{0.5}$, where Re is the Reynolds Number.

TIT helically coiled tube heat exchanger consists of two helically shaped tubes, which are concentric in nature. The details of geometry and its dimensions are as shown in Tables 1 and 2. Fig. 2 shows the different configurations of the inner tube. Cold fluid flows in the annulus and the hot fluid flows in the inner tube. The flow configuration considered for the present study is counter flow.

An independence mesh analysis has been carried out and each of the geometries was evaluated with different mesh sizes. The calculated numerical results are shown in Fig. 3, and they agree with [18]. According to the numerical results as shown in Fig. 3, element size greater than 25x 10^6 does not affect Nusselt Number. Mesh independence test has been carried out for individual geometry and mesh sizes are plotted in Fig. 3. In order to perform the CFD analysis, the polyhedral mesh was generated on a helically shaped tube. The simulation geometry was generated using ANSYS Workbench 18.1 and meshes were generated in Altair Hyper Mesh 13.0.

Table 1
Geometry details.

Parameters	Inner Tube	Outer Tube
External diameter (m)	0.026	0.0508
Helical diameter (m)	0.77	0.77
Pitch (m)	0.1	0.1
Velocity (m/s)	0.01	0.038–0.068
Dean number (dimensionless)	200	200–400
Prandtl number (dimensionless)	7	7

Table 2
Geometry with different shaped tubes.

Geometry	Design Modification
A	Circular Tube
B	Square Tube
C	Ellipse Tube
D	Pentagon Tube
E	Hexagon Tube

The mesh density was made to improve from 0.038617 cellsm^{-3} to 8×10^6cellsm^{-3}. The mesh selection for all geometries is in the range between 17.5×10^6 and 24×10^6, with the intension of error lesser than 1%. Mesh independence study was carried out for individual geometries as shown in Fig. 3 using different Nusselt Number. The mesh elements do not cause any error to the results when the element numbers are greater than 20×10^6.

SIMPLE scheme has been used for Pressure-velocity coupling. Momentum equation has been detached by QUICK scheme. The simulations were carried out by applying the accuracy level of 1.0e^{-04} and1.0e^{-06} in continuity and momentum equations respectively. The post-processing is carried out using CFD-Post 18.1 which provides the contours of different configurations with

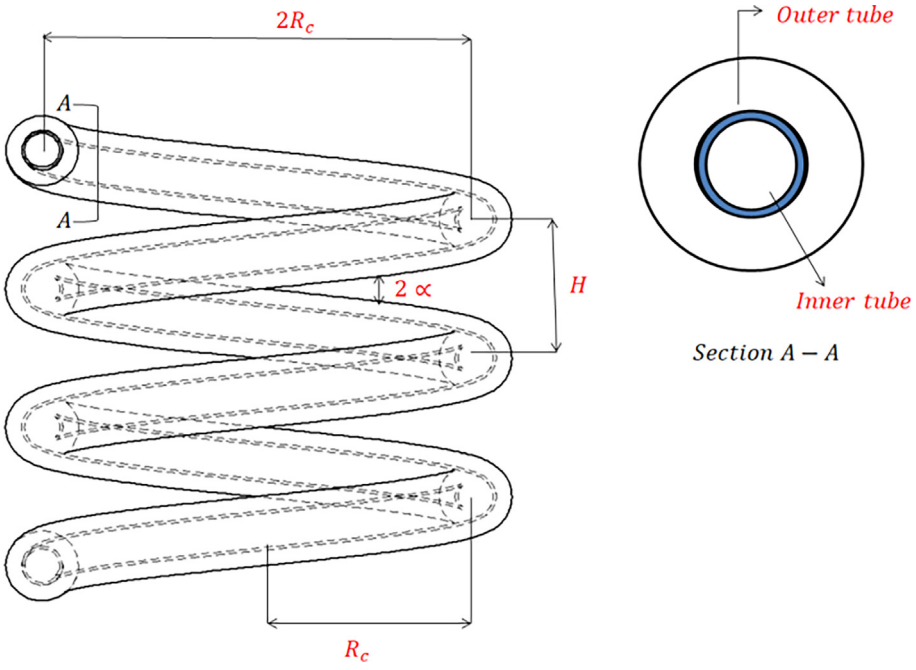

Fig. 1. Geometry of a helical pipe.

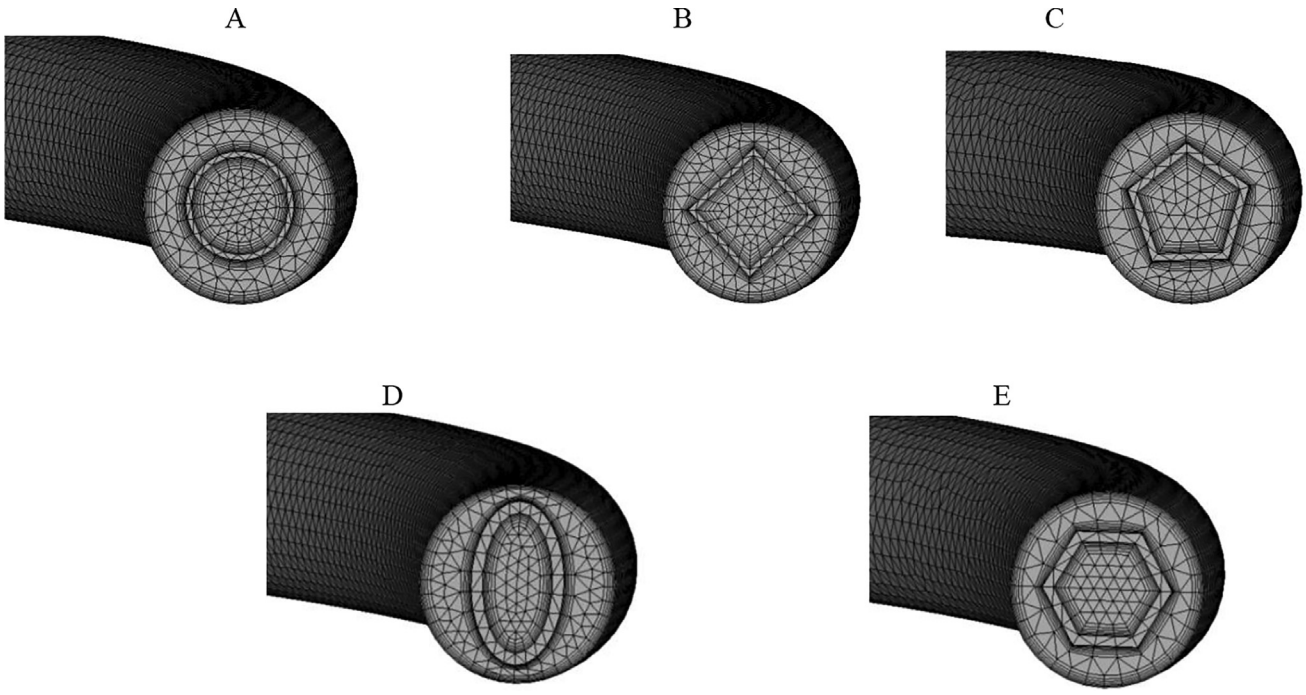

Fig. 2. Polyhedral mesh for different modified shaped tubes.

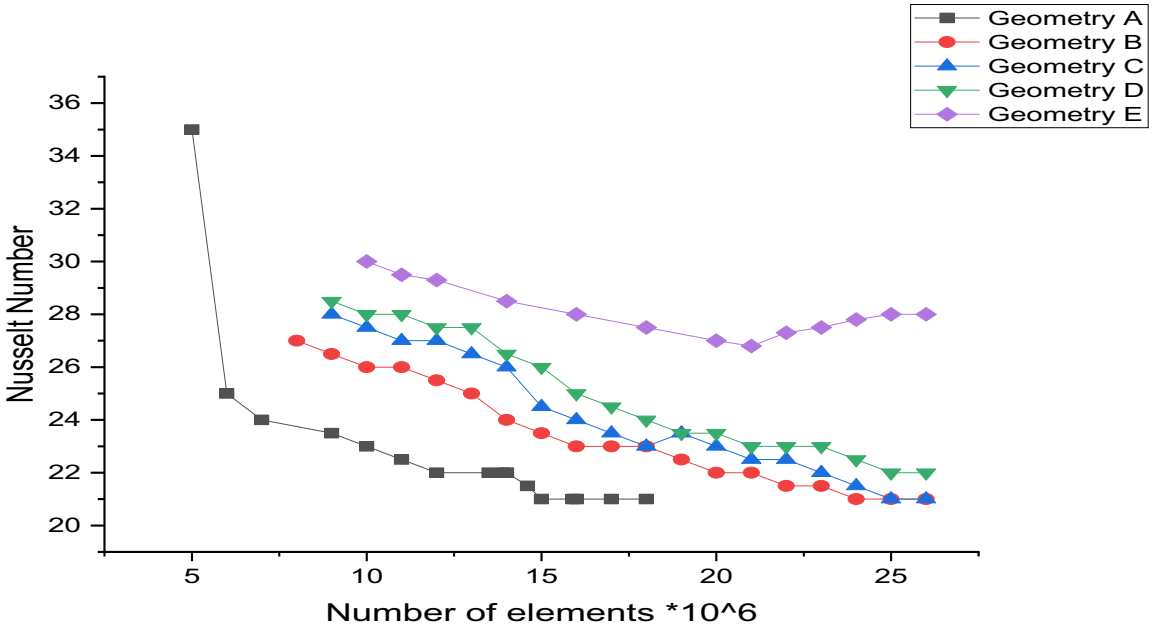

Fig. 3. Mesh independence study.

respect to the thermal parameters, animation, and angular positions of the helical tube.

The selection of temperature at the inlet to the inner tube and outer tube is 300 K and 380 K respectively. The constant velocity boundary condition is applied at the inlet to the inner tube. Computations were carried by varying the Dean Number from 200 – 400 respectively. The computations were carried out at convergence criterion of continuity up to10^{-4}. The number of iterations was carried out up to 1000. The Dean number is calculated using eq. (1)

$$De = \frac{\rho v D_h}{\mu}\sqrt{\delta} \quad (1)$$

Where ρ represents density, v represents velocity in m/s, μ is the dynamic viscosity, and D_h is the hydraulic diameter which is given by eq. (2) and δ is the curvature ratio given in eq. (3).

$$D_h = \frac{4A}{P} \quad (2)$$

Where P is the perimeter of the coil and A is the cross-sectional area.

Curvature ratio, δ:

$$\delta = \frac{d_o}{D_c} \quad (3)$$

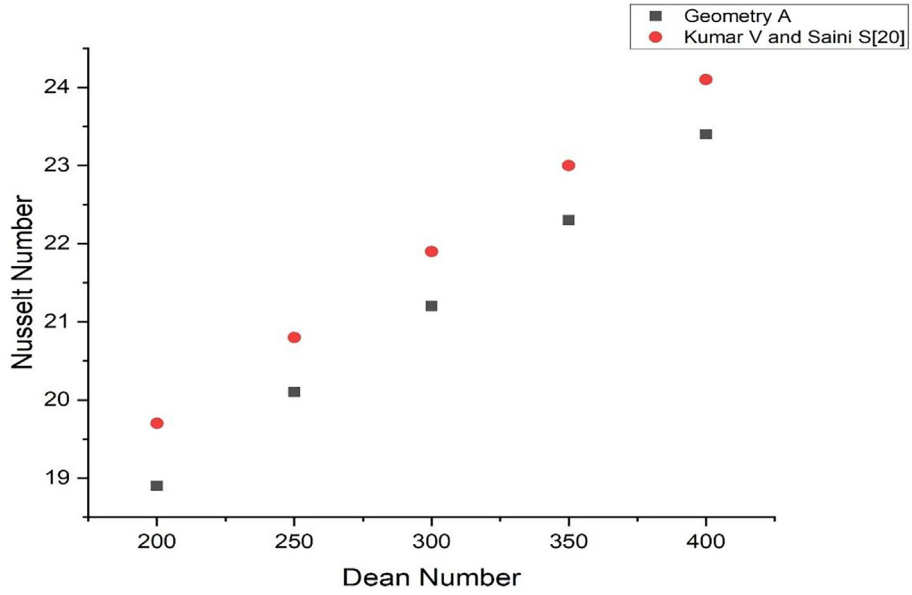

Fig. 4. Nusselt number versus Dean Number.

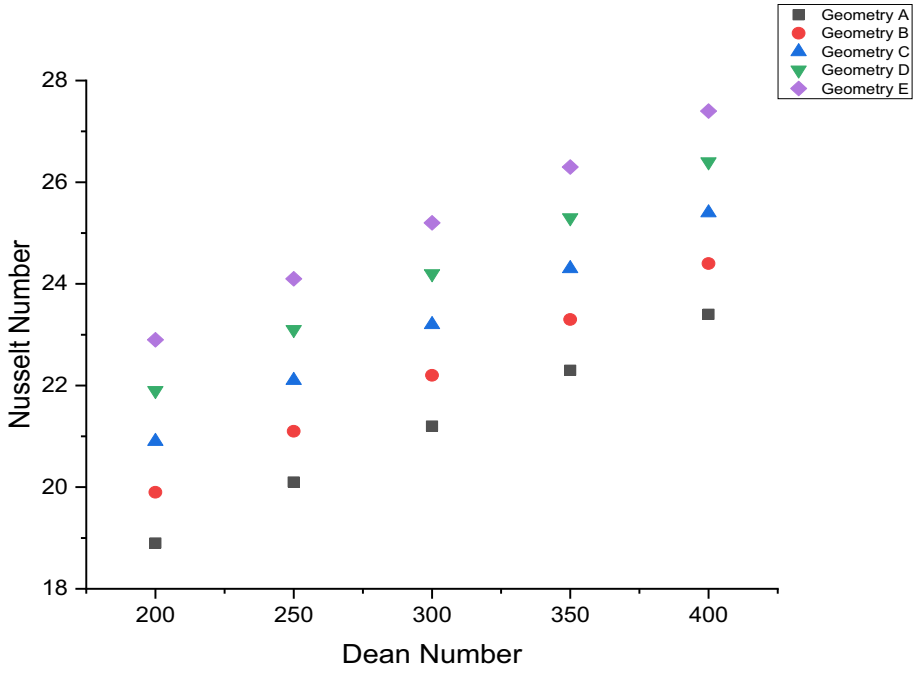

Fig. 5. Variation of Nusselt number with Dean Number.

where d_o and D_c are the outer diameter of the inner tube and helical diameter respectively.

Differential equations govern laminar flow has been written in the vector form as shown in eqs. (4–7).

Continuity equation:

$$\frac{\partial \rho u_i}{\partial x_i} = 0 \tag{4}$$

Momentum equation:

$$\frac{\partial(\rho u_i u_j)}{\partial x_j} + \frac{\partial P}{\partial x_i} - \frac{\partial}{\partial x_j}\left[(\mu + \mu_t)\left(\frac{\partial u_i}{\partial x_j} + \frac{\partial u_j}{\partial x_i}\right)\right] - F_i = 0 \tag{5}$$

Energy equation:

$$\frac{\partial(\rho E_{uj})}{\partial x_j} + \frac{\partial(P u_j)}{\partial x_j} - \varnothing - \frac{\partial}{\partial x_j} k\left(\frac{\partial T}{\partial x_j}\right) = 0 \tag{6}$$

Where $\varnothing$ is the viscous heating, it is shown in eq. (7).

$$\varnothing = \mu \frac{\partial u_i}{\partial x_j}\left(\frac{\partial u_i}{\partial x_j} + \frac{\partial u_j}{\partial x_i}\right) \tag{7}$$

The thermophysical properties of fluid were calculated using the bulk mean temperature, which is defined by:

For hot fluid:

$$T_{bh} = \frac{T_{hi} + T_{ho}}{2} \tag{8}$$

For cold fluid:

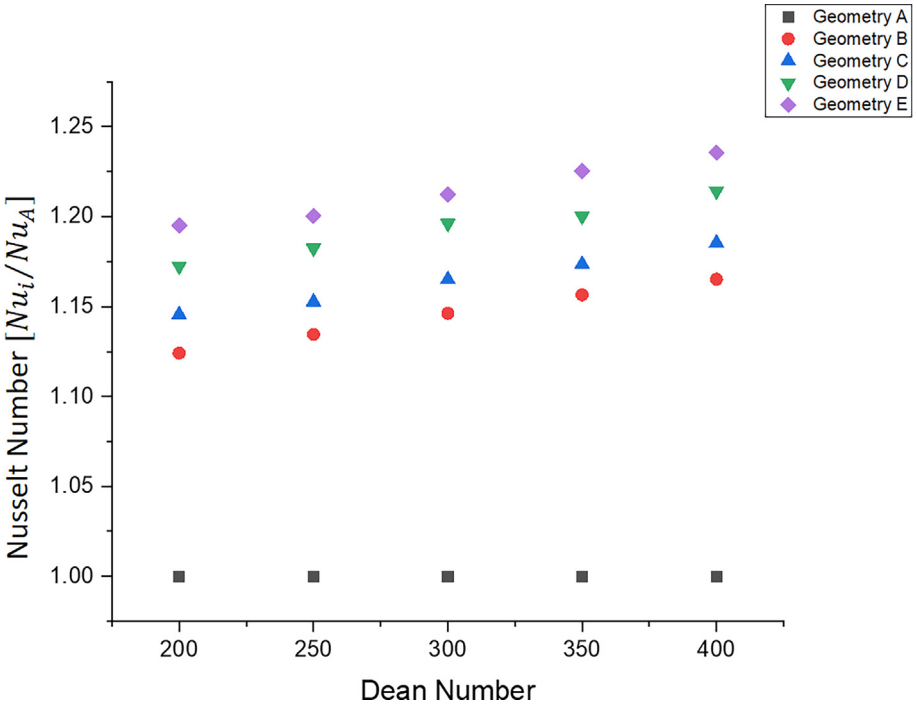

Fig. 6. Comparison of Nusselt number for individual geometries.

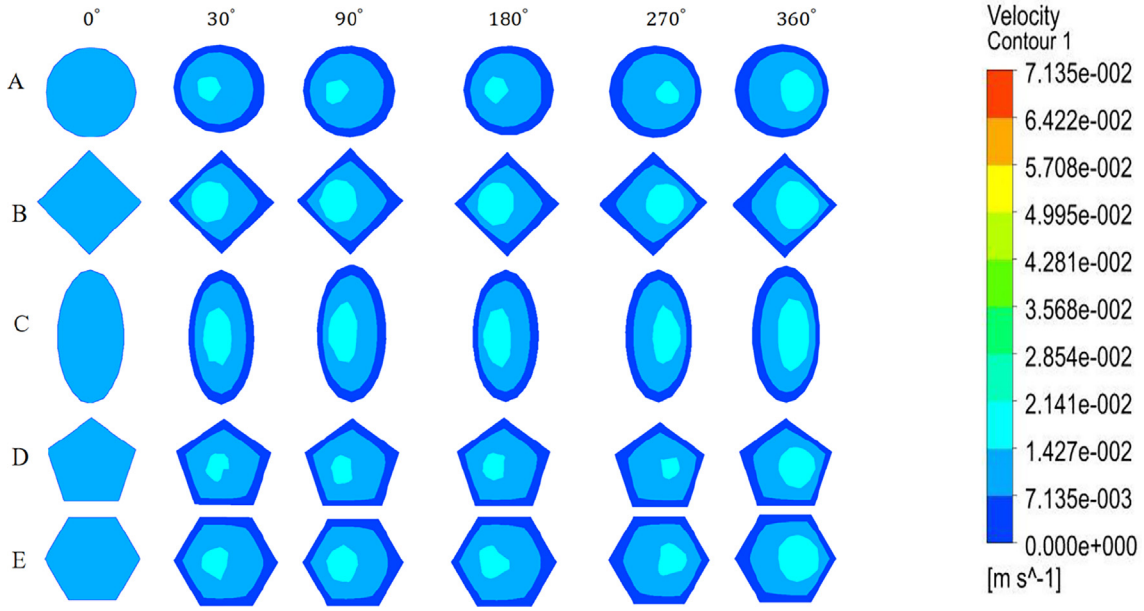

Fig. 7. Velocity contours of the inner tube of different models of TIT helically coiled heat exchanger.

$$T_{bc} = \frac{T_{ci} + T_{co}}{2} \tag{9}$$

Where T_{bh} is the average temperature of hot fluid and T_{bc} is the bulk mean temperature of cold Fluid.

The convective heat transfer rate of cold fluid is determined by using Eq. (10).

$$Q_c = \dot{m}_c C_{pc}(T_{co} - T_{ci}) = h_o A_o(\overline{T_w} - T_{bc}) \tag{10}$$

Where $\overline{T_w}$ is the inner tube average wall temperature.

The average heat transfer rate and overall heat transfer coefficient based on the inner tube is evaluated by using Eqs. (11) and (12) respectively.

$$Q_{ave} = \frac{Q_h + Q_c}{2} \tag{11}$$

$$Q_{ave} = U_i A_i \Delta T_{LMTD} \tag{12}$$

Where ΔT_{LMTD} is the logarithmic mean temperature.

The thermal resistance of the system is expressed as:

$$\frac{1}{U_i A_i} = \frac{1}{h_i A_i} + \frac{\ln\left(\frac{d_o}{d_i}\right)}{2\pi k_p l} + \frac{1}{h_o A_o} \tag{13}$$

The convective heat transfer coefficient of the internal pipe (h_i) is determined by calculating eq. (14).

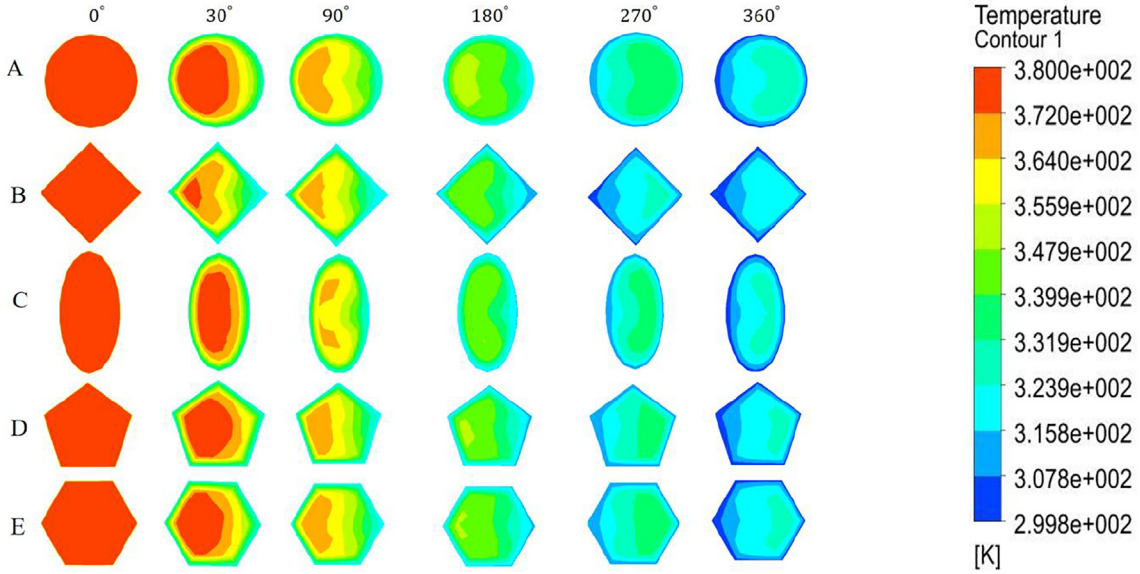

Fig. 8. Temperature contours of internal tube for different models of TIT helically coiled heat exchanger.

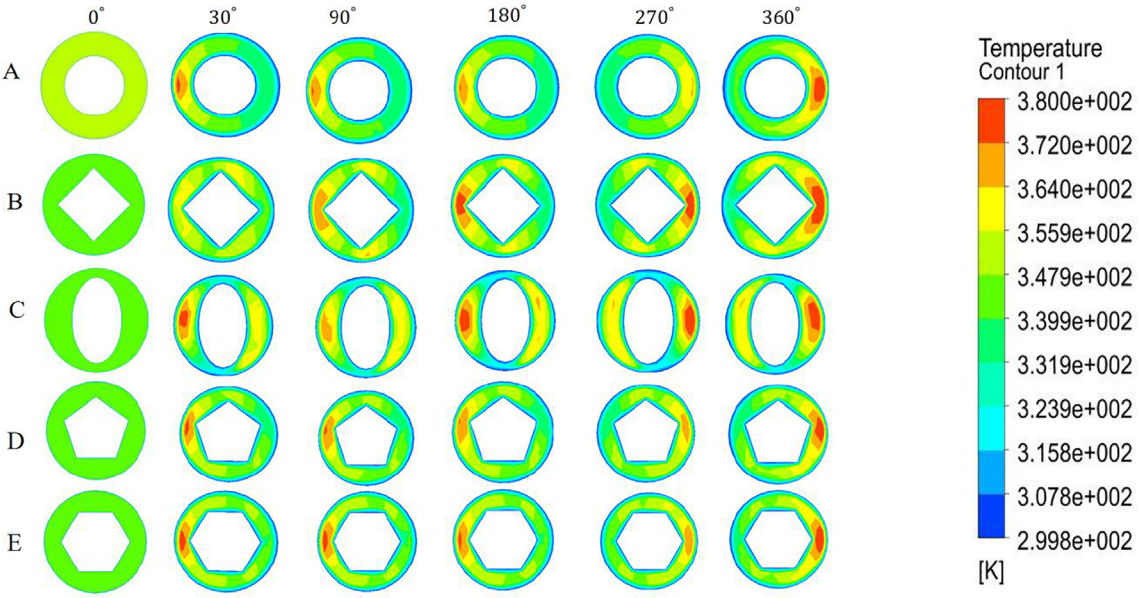

Fig. 9. Temperature contours in the annulus zone.

$$h_i = \frac{1}{\left[\frac{1}{U_i} - \frac{d_i \ln\frac{d_o}{d_i}}{2k_p} - \frac{d_i}{d_o h_o}\right]} \quad (14)$$

Nusselt number is determined using Eq. (15).

$$N_u = \frac{h_i d_i}{k_i} \quad (15)$$

By using Darcy–Weisbach friction factor can be calculated:

$$f = \frac{2\Delta P D_h}{\rho v^2 l} \quad (16)$$

Effectiveness of heat exchanger is given by Eq. (17)

$$\in = \frac{m_h C_h (T_{hi} - T_{ho})}{mC_{min}(T_{hi} - T_{ci})} \quad (17)$$

Where $T_{hi}$and T_{ho} are inlet and outlet temperature of hot fluid respectively.

T_{ci} is the inlet temperature of cold fluid.

3. Results and discussion

The numerical results in the present study are verified with the results of [20]. Fig. 4 shows the variation of Nusselt number versus Dean number for Geometry A. The results show that the numerical results of geometry A and experimental data reported by [20] tend to be the same. Fig. 5 shows the variation of Nu with Dean number. Fig. 6 shows the relationship between the Nusselt number of different geometries and circular tube. It is clear from Fig. 6 that there is a rise in Nusselt number as the Dean number increases. And it is evident from Fig. 6 that Nusselt number is raised 1.125, 1.145,

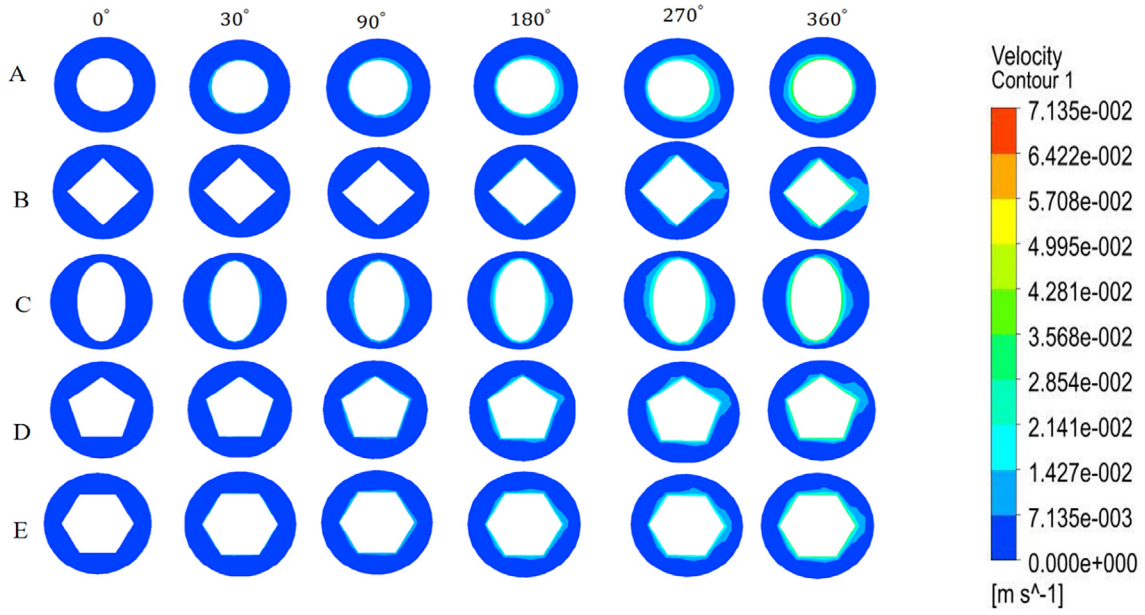

Fig. 10. Velocity contours for the external pipe of different models of TIT helically coiled heat exchanger.

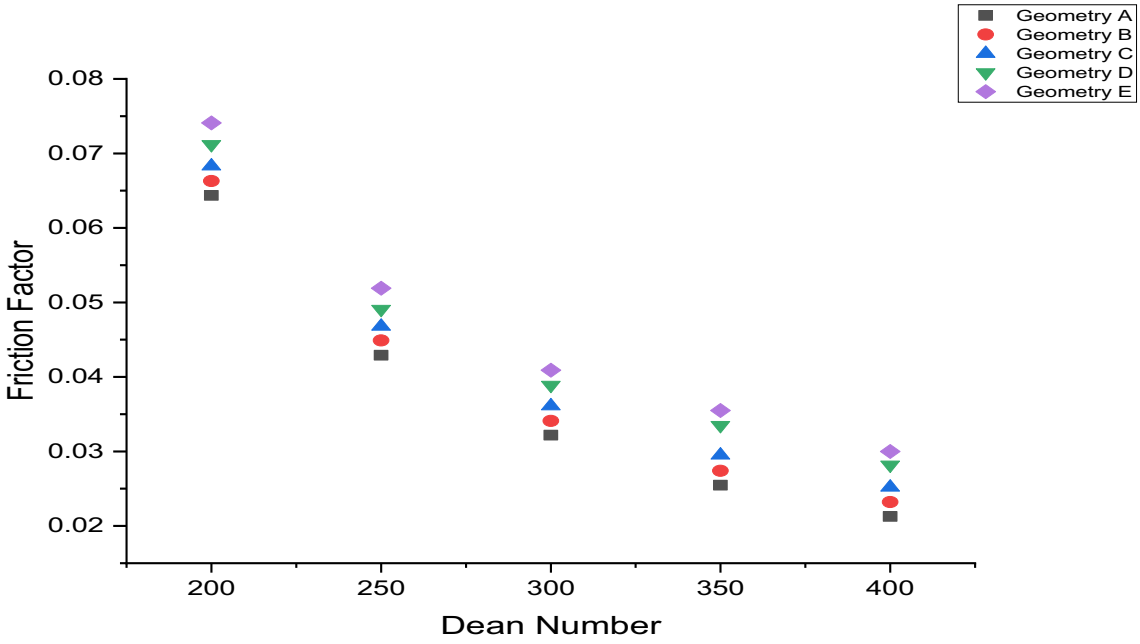

Fig. 11. Friction factor versus Dean number.

1.175, and 1.2 times as compared to the plain tube at a Dean number of 200. Fig. 7 represents the velocity contours for the inner tube of five different geometries of the TIT helically coiled heat exchanger. Rows represent the different geometry of the TIT helically coiled heat exchanger. The columns show different cross-section (0°, 30°, 90°, 180°, 270°, and 360°). It is observed from the figure that the modified geometries i.e. from B to E, the contours of velocity changes at 30° position and recognizing different profiles of velocity. However, from 90° to 360° slight changes in the profile (patterns) have been observed. The pattern of velocity is proof of the total development of the fluid flow. For the geometries, A, B, C, D, and E, the maximum value of velocity is observed towards the surface of the outside tube.

Fig. 8 represents the contours of the temperatures in the inner pipe for the different configuration of TIT helically coiled heat exchanger. The maximum values of temperature are observed towards the outside of the tube, due to the generation of the vortex. Fig. 8 also signifies an increase of the patterns for the angular positions 30° to 360° due to more surface area. Fig. 9 represents the velocity contours in the annulus. For the geometries from (B) to (E), it is enough to confirm that there is a developed fluid flow in the annulus.

Fig. 10 illustrates the temperature contours in the annulus zone. It is noticed that there is a significant rise in temperature in the annulus at an angular position of 360°. For models from B to E, the temperature amplified uniformly and there are no significant

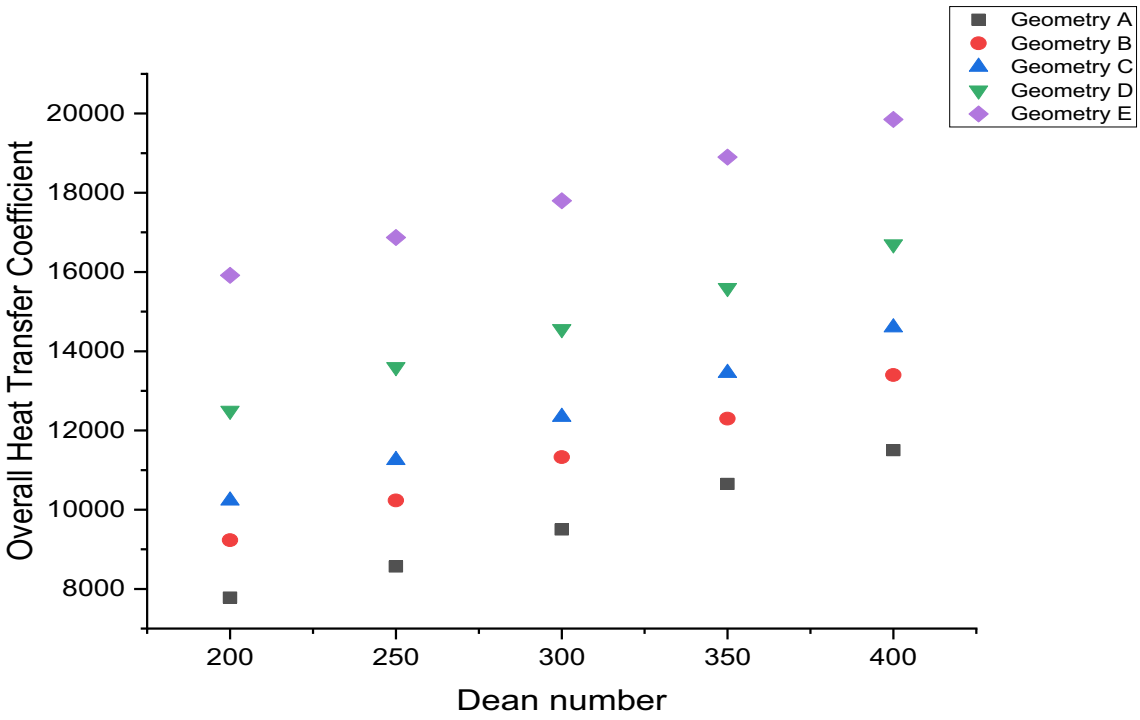

Fig. 12. Overall heat transfer coefficient versus Dean number.

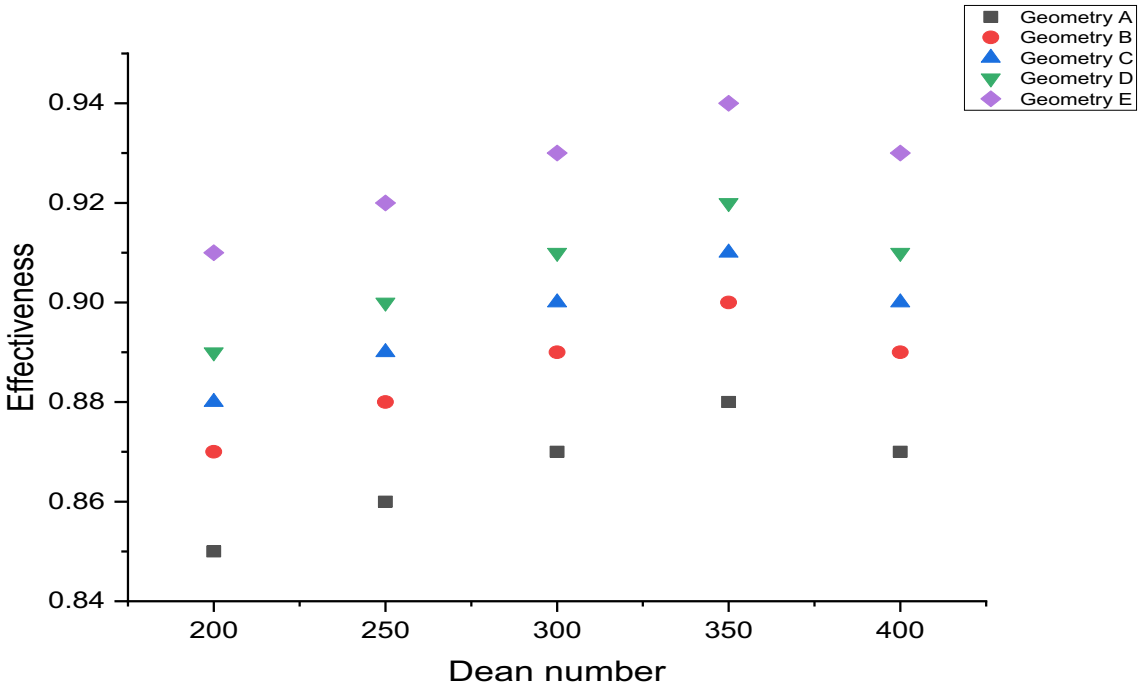

Fig. 13. Effectiveness versus Dean number.

temperature differences among the models. Figs. 5 to 10 provides the proof of an increase in Nusselt Number subjected to Dean Number. The increase of heat transfer from geometry A to E is due to the passive technique, better surface area, and centrifugal force. Fig. 11 shows the prediction of numerical results of Darcy–Weisbach friction factor with respect to Dean Number. It is observed in Fig. 11 that there is a decrease in the frictional factor as the Dean number increases. The decrease in frictional factor indicates a drop in pressure drop since both are directly proportional. This depletion is due to the perimeter and number of edges of the geometry as compared with the circular tube. When compared to Geometry B to C, the frictional factor is increased by 7.94%. As the surface area is better enough (Geometry D and E) friction factor gradually increases by 3.56%. In the case of Geometry C to D, the friction factor is increased by 7.25%. Fig. 12 shows the variation of the overall heat transfer coefficient with Dean Number.

As expected overall heat transfer coefficient increases with the Dean Number. For the geometries from B to E the value of the overall heat transfer coefficient is more as compared with the circular tube. Fig. 13 shows the variation of Effectiveness with Dean number. It is clear from the figure that effectiveness is a function of Dean Number. At larger Dean Number the effectiveness decreases.

4. Conclusions

A numerical study has been performed to investigate heat transfer and friction factor of fluid flow in the annulus region of a tube in tube helical heat exchanger for the laminar regime at different Dean Numbers. The behaviour of the overall heat transfer coefficient under the influence of different cross-sections of the inner pipe of the heat exchanger revealed that effectiveness and overall heat transfer coefficient was strongly affected with Dean Number. The use of different geometry of the inner pipe of the tube in tube helical heat exchanger causes a higher friction factor at low Dean Number. The Nusselt Number for Geometry B to E is greater than that of a circular tube and was found to increase with Dean Number. The use of geometry E increases the Nusselt number and friction factor by 17.05% and 15% respectively at a Dean number of 400 as compared with a circular tube. Nusselt number of Geometry B increases by 13.73% as compared to Geometry A. It is observed that the increase in Nusselt number from Geometry B to C is 1.45% and geometry C to E is 3.24%.

CRediT authorship contribution statement

N. Sreenivasalu Reddy: Conceptualization, Methodology. **S. Gowreesh Subramanya:** Writing - original draft. **K.C. Vishwanath:** Investigation. **S. Kanchiraya:** Software, Validation. **V. Satheesha:** Supervision. **M. Karthikeyan:** Writing - review & editing.

Declaration of Competing Interest

The authors declare that they have no known competing financial interests or personal relationships that could have appeared to influence the work reported in this paper.

Acknowledgements

The authors would like to gratefully acknowledge the support of the management of Rajarajeswari group of institutions (RRGI) for this original research work.

References

[1] M. Ciofalo, A. Arini, M. Di Liberto, On the influence of gravitational and centrifugal buoyancy on laminar flow and heat transfer in curved pipes and coils, Int. J. Heat Mass Transf. 82 (2015) 123–134, https://doi.org/10.1016/j.ijheatmasstransfer.2014.10.074.

[2] H. Saffari, R. Moosavi, N.M. Nouri, C.-X. Lin, Prediction of hydrodynamic entrance length for single and two-phase flow in helical coils, Chem. Eng. Process. Process Intensif. 86 (2014) 9–21, https://doi.org/10.1016/j.cep.2014.10.005.

[3] M.R.H. Nobari, B. Shiniyan, M. Mirzaei, Mixed convection in a vertical helical annular pipe, Int. J. Heat Mass Transf. 73 (2014) 468–482, https://doi.org/10.1016/j.ijheatmasstransfer.2014.01.068.

[4] L. Guo, Z. Feng, X. Chen, An experimental investigation of the frictional pressure drop of steam–water two-phase flow in helical coils, Int. J. Heat Mass Transf. 44 (14) (2001) 2601–2610, https://doi.org/10.1016/S0017-9310(00)00312-4.

[5] L. Zhao, L. Guo, B. Bai, Y. Hou, X. Zhang, Convective boiling heat transfer and two-phase flow characteristics inside a small horizontal helically coiled tubing once-through steam generator, Int. J. Heat Mass Transf. 46 (25) (2003) 4779–4788, https://doi.org/10.1016/S0017-9310(03)00354-5.

[6] H.M. Ju, Z.Y. Huang, Y.H. Xu, B. Duan, Y. Yu, Hydraulic performance of small bending radius helically coil-pipe hydraulic performance of small bending radius helically coil-pipe, J. Nuci. Technol. 38 (2001) 826–831.

[7] R.C. Xin, A. Awwad, Z.F. Dong, M.A. Ebadian, An experimental study of single-phase and two-phase flow pressure drop in annular helicoidal pipes, Int. J. Heat Fluid Flow 18 (5) (1997) 482–488, https://doi.org/10.1016/S0142-727X(97)80006-9.

[8] R.C. Xin, A. Awwad, Z.F. Dong, M.A. Ebadian, H.M. Soliman, An investigation and comparative study of the pressure drop in air-water two-phase flow in vertical helicoidal pipes, Int. J. Heat Mass Transf. 39 (4) (1996) 735–743, https://doi.org/10.1016/0017-9310(95)00164-6.

[9] A. Awwad, R.C. Xin, Z.F. Dong, M.A. Ebadian, H.M. Soliman, Measurement and correlation of the pressure drop in air-water two-phase flow in horizontal helicoidal pipes, Int. J. Multiph. Flow 21 (4) (1995) 607–619, https://doi.org/10.1016/0301-9322(95)00011-L.

[10] A.B. Biswas, S.K. Das, Two-phase frictional pressure drop of gas–non-Newtonian liquid flow through helical coils in vertical orientation, Chem. Eng. Process. Process Intensif. 47 (5) (2008) 816–826, https://doi.org/10.1016/j.cep.2007.01.030.

[11] L. Santini, A. Cioncolini, C. Lombardi, M. Ricotti, Two-phase pressure drop in a helically coiled steam generator, Int. J. Heat Mass Transf. 51 (2008) 4926–4939, https://doi.org/10.1016/j.ijheatmasstransfer.2008.02.034.

[12] M. Colombo, L.P.M. Colombo, A. Cammi, M.E. Ricotti, A scheme of correlation for frictional pressure drop in steam–water two-phase flow in helicoidal tubes, Chem. Eng. Sci. 123 (2015) 460–473, https://doi.org/10.1016/j.ces.2014.11.032.

[13] G.F.C. Rogers, Y.R. Mayhew, Heat transfer and pressure drop in helically shaped coiled tube with turbulent flow, Int. J. Heat Mass Transf. 7 (1964) 1207–1216.

[14] X.F. Liu, G.D. Xia, G. Yang, Experimental study on the characteristics of air–water two-phase flow in vertical helical rectangular channel, Int. J. Multiph. Flow 73 (2015) 227–237, https://doi.org/10.1016/j.ijmultiphaseflow.2015.03.012.

[15] Y. Murai, S. Yoshikawa, S.I. Toda, M.A. Ishikawa, F. Yamamoto, Structure of air-water two-phase flow in helically coiled tube, Nucl. Eng. Des. 236 (2006) 94–106, https://doi.org/10.1016/j.nucengdes.2005.04.011.

[16] J.S. Jayakumar, S.M. Mahajani, J.C. Mandal, P.K. Vijayan, Experimental and CFD analysis of heat transfer in helically coiled heat exchanger, Chem. Eng. Res. Des. 86 (3) (2008) 221–232, https://doi.org/10.1016/j.cherd.2007.10.021.

[17] C. Pan, J. Wang, CFD analysis of heat transfer for oscillation flow in helically coiled tube heat-exchanger, Comput. Chem. Eng. 69 (2014) 59–65, https://doi.org/10.1016/j.compchemeng.2014.07.001.

[18] K. Sharifi, M. Sabeti, M. Rafiei, A.H. Mohammadi, L. Shirazi, Computational fluid dynamics (CFD) technique to study the effects of helical wire inserts on heat transfer and pressure drop in a double pipe heat exchanger, Appl. Therm. Eng. 128 (2018) 898–910, https://doi.org/10.1016/j.applthermaleng.2017.08.146.

[19] H. Ju-Lee, J. Ryu, S. Hyuk-Lee, Influence of Performated Fin on Flow Characteristics and Thermal Performance in Spiral Finned-Tube Heat Exchanger, Energies 12 (2019) 556, https://doi.org/10.3390/en12030556.

[20] V. Kumar, S. Saini, M. Sharma, K.D.P. Nigam, Pressure drop and heat transfer study in tube-in-tube helical heat exchanger, Chem. Eng. Sci. 61 (13) (2006) 4403–4416, https://doi.org/10.1016/j.ces.2006.01.039.

[21] M.A. Omara, Mohamed A, Abdellatif, Nigam, Experimental study of heat transfer and friction factor inside elliptical tubes fixed with helical coils, Appl. Therm. Eng. 134 (2018) 407–418, https://doi.org/10.1016/j.applthermaleng.2018.02.017.

[22] S.K. Naghibzadeh, M.R. Hajmohammadi, M. Saffar-Avval, Heat transfer enhancement of a nanofluid in a helical coil with flattened cross-section, Chem. Eng. Res. Des. 146 (2019) 36–47, https://doi.org/10.1016/j.cherd.2019.03.008.

[23] S.W. Chang, P.-S. Wu, W.L. Cai, J.H. Liu, Turbulent flow and heat transfer of helical coils with twisted section, Appl. Therm. Eng. 180 (2020) 115919, https://doi.org/10.1016/j.applthermaleng.2020.115919.

Experimental Investigation of Forced Convection Heat Transfer from Vertical Grooved Plates

[1]Abdul Razak Kaladgi, [2]Vishwanath K C, [3]Sreenivasalu Reddy
[4*]Chandrashekar A

[1]Department of Mechanical Engineering, P.A. College of Engineering, Mangalore – 574153, Karnataka
[2, 3] Department of Mechanical Engineering, RajaRajeswari College of Engineering, Bangalore-560074, Karnataka
[4]Department of Mechanical Engineering, Bangalore Institute of Technology, Bangalore – 560004, Karnataka
*Correspondence: acsmech@gmail.com

Abstract: Increasing the heat transfer rate has become prime task in electronic industry because of miniaturization of equipments. Recently many investigators carried out numbers of experiments for achieving maximum heat transfer rate, the present investigation mainly focus on increasing the thermal dissipation from the surface by providing grooves over the surface of aluminum plates with various ranges of length to width ratio and length to depth ratio. The experiment was carried out for varying Reynolds number and varying the amount of heat flux given to the plate. It has been observed that variation in L/D ratio and flow rate affects the heat transfer rate and friction factor.

Keywords: Nano fluids; Heat flux; Groove flat plate, air, Reynolds number, heat transfer coefficient.

1. Introduction

Plates have received considerable attention because of the fact that they have been used widely in industrial applications. They have found extensive use in heat exchangers. When improvement in the process of heating or cooling is required, then better design of plate compactness and spatial geometry is very essential. The use of heat transfer enhancement has become widespread during the last 50 years. The goal of heat transfer enhancement is to reduce the size and cost of heat exchanger equipment, or increase the heat duty for a give size heat exchanger. This goal can be achieve in two ways: active and passive enhancement. Of the two, active enhancement is less common because it requires addition of external power to cause a desired flow modification. On the other hand, passive enhancement consists of alteration to the heat transfer surface or incorporation of a device whose presence results in a flow field modification. One of the popular enhancements is the introduction of grooves on the surface of the heat exchanger. The apparent advantages of grooved plates are that they increase the heat transfer rate by providing additional surface area.

Inspite of the above facts, only a very few studies have been reported in the literature on the flat plate with grooves.

Ashish Dixita & Anil Kumar Patila [1] carried out an experimental study on different types of grooves which were made on the extended surfaces. They found that the heat transfer was more for fins having inclined grooves. Chang, S. W., Su, L. M., Yang, T. L., and Chiou, S. F [2] made an experimental study on fin channels having 900 staggered ribs and developed correlation to study the influence of Reynolds number and L/B on heat transfer, also suggested the optimum length to gap ratio that results in increased heat flux. The increment in heat transfer was up to 140–200 % using 90° staggered ribs. Kadir Bilen, Murat Cetin, Hasan Gul, Tuba Balta [3] conducted an experiment on tubes having grooves of different geometry. The ratio L/D was fixed in their study. They mainly developed a correlation for heat transfer and friction factor. The results of their study revealed that heat transfer enhancement does occur for tubes having grooves as compared with tubes without grooves. Faheem Akthar, Abdul Razak R Kaladgi and

Mohammed Samee A Dafedar [4] conducted an experimental investigation of the natural convection heat transfer over circular dimpled surfaces .The arrangement was inline. The various heat transfer parameters considered were Nusselt number, heat transfer coefficient and heat transfer rate. They concluded that heat transfer enhancement occurs for the dimpled surfaces as compared to flat plates. In an another study, Amjad Khan, Mohammed Zakir Bellary, Mohammad Ziaullah, Abdul Razak Kaladgi [5] carried out an experimental study on plates having dimples of circular shapes. The analysis was carried out for different arrangements like centrally increasing the diameter of dimples in the direction of flow; centrally decreasing the diameter of dimples in the direction of flow etc. They concluded that heat transfer enhancement does occur for plates having dimples but at the cost of pressure drop. N. K. Ghaddar, K. Z. Korczak, B. B. Mikic, A.Y. Patera [6], numerically studied the heat transfer characteristics in the channels having grooves on one plate. They solved the Navier-stokes and energy equations numerically and showed complex flow patterns of flow recirculation flow separation etc. Tang xinyi and zhu dongsheng [7] conducted experimental and computational study (using software) on rectangular channels having ribs and grooves. They used the SST turbulence model to solve the equations and carry out the simulations. They found that the Nu ratio and Cf were more for the channels having ribs and grooves as compared to the channels having only ribs. Apurba Layek, J. S. Saini, S. C. Solanki [8], carried an experiment to study the effect of heat transfer on a duct having ribs and grooves on one surface. They observed an increment in the Nusselt number by about 3.24 times as compared to smooth surface. Ali Najah Al-Shamani, K. Sopian, H. A. Mohammed, Sohif Mat, Mohd Hafidz Ruslan, Azher M. Abed [9] computationally studied heat transfer characteristics of a channel having ribs and grooves on one wall. They used the STD K-epsilon turbulence model to solve the governing equations. They carried the investigation on various ribs and groove combination. They also used different nano fluids with different concentrations. They found that trapezoidal rib groove of good height gives the maximum heat transfer rate. Smith Eiam-saard and Pongjet Promvonge [10] conducted an experiment to study heat transfer characteristics in a duct using 3 types of groove and rib combination. They found an increment in the heat transfer as compared to smooth duct.

2. Experimental Setup

A forced convection apparatus was adapted for this study. Figure 1 show the experimental set up used for the present study. It consists of a rectangular duct to keep the grooved plates, a blower to supply air. The air from blower passes through a flow passage consisting of pipes and finally through the rectangular duct, orifice meter was used to measure flow rate through the passage, a band heater placed inside the duct heats the air and is controlled by dimmer start. Temperature of the air at inlet and outlet were measured using thermocouples.

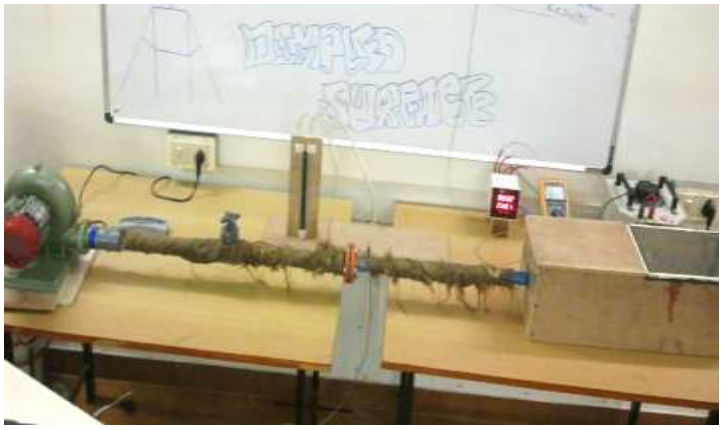

Figure.1: Experimental set up

The experimental set-up consists of following instruments: -

- Dimmer stat (0-250 Volt AC Supply)
- Voltmeter (0 - 400 Volt)
- Ammeter (0 - 10 Ampere)
- Digital Temperature Indicator of 8 channels (Range 0oC – 400 oC)
- Calibrated k-type Thermocouples
- Four Test Plates
- Orifice plate, manometer, Blower (13000 rpm)

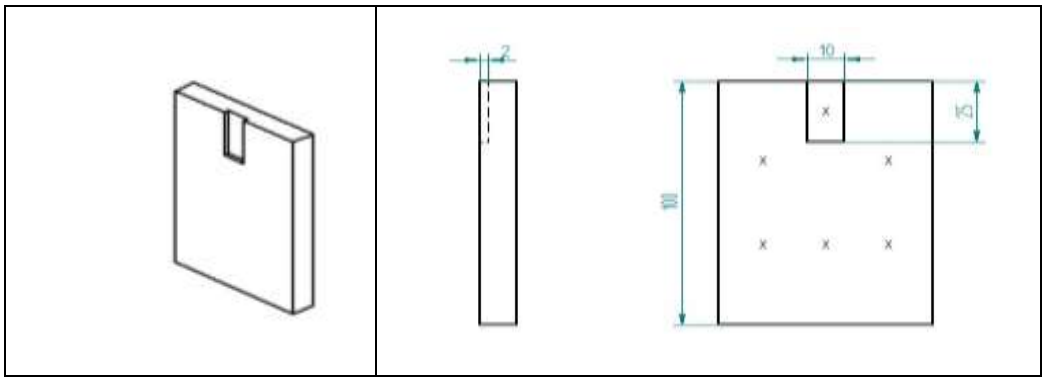

Fig. 2a: Schematic diagram of plate 1 with location of thermocouples (Shown by cross)

Fig. 2b. Schematic diagram of all the plates

The test plates were made of aluminium and rectangular grooves of different lengths of 25 mm, 50 mm, 75 mm, and 100 mm were made onto each of them. The dimension of the plate is 100 mm in length, 60 mm in breadth and 10mm in thickness. The groove breadth is 10 mm. Figs. 2a and 2b shows the schematic diagram of the plates used for the present study.

The cross symbol (X) in figure 2a shows the measurement points of the temperature. The measurement points on the surface of the plate other than the groove were positioned in an equal distance from both top and bottom of the plate. The temperature measurement points in the groove were placed in an equidistant manner according to the groove length. Thermocouples (k-type) were used to measure the temperature. The test plates are fixed onto a wooden box with the groove side open to atmosphere. The wooden box itself acts as an insulator, is filled with glass wool (insulator), in which the strip heater is held. The rectangular plate is kept on the wooden box such that the back side is on the heater and front side open.

3. Results and Discussion

The aim of the experiment is to measure the temperatures along the surface of the plate for the desired constant heat flux (The heater is adjusted for the desired power input with the help of

dimmer stat). The experiment is allowed to run till the steady conditions are reached, and the temperature reading was noted.

The parameters varied during the experimentation were:

(i) Heat Input: The experiment were carried out for different heat inputs.

(ii) Aspect ratio: The length of the groove to the width of the groove is altered during the experiment.

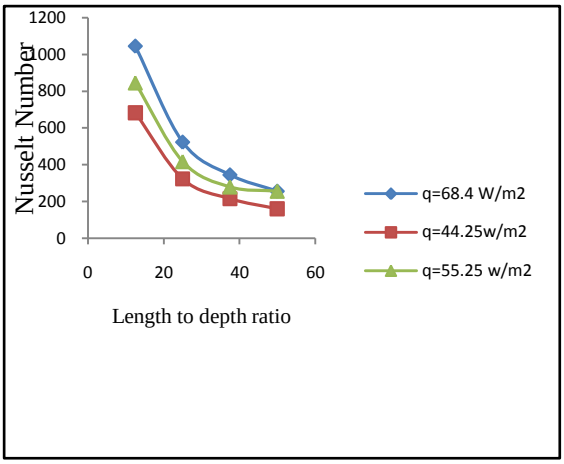

Figure 3.:Nusselt's number Vs of L/D ratio

Figure 3 shows the effect of length to depth ratio on Nusselt number of the plate. The results were plotted for different heat flux conditions. It was observed that Nusselt number increases as the size of groove decreases due to direct flow impingement on the downstream boundary and strengthened flow mixing by vortices at the downstream [11,12]. The formation of vortex pairs periodically shedding off from the grooves, a large up wash regions with some fluids coming out from the central regions of the grooves are the main causes of enhancement of Nusselt number & is more pronounced near the downstream rims of the dimples [13].

Figure 4 shows the variation of Nusselt number for different discharges. It can be seen that Nusselt number increases, as the value of discharge increases as expected & hence increases the heat transfer coefficient. This may be attributed to the fact that due to increased flow rates, the velocity increases and hence increases the heat transfer rate of the plate. It can also be observed that the Nusselt number is highest for L/D ratio of 12.5 and lowest for L/D ratio of 50. So length of the groove affects significantly the heat transfer rate.

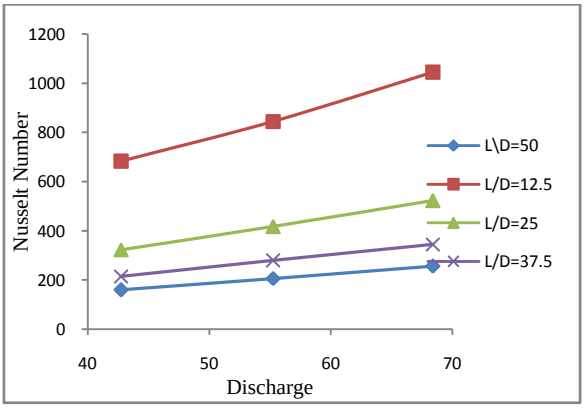

Figure.4: Nusselt vs. Discharge

The Figure 5 shows the variation of heat transfer coefficient with Reynolds number for an L/D ratio of 12.5. From the figure we can say that as the Reynolds number increases, the

heat transfer coefficient increases as expected, because at high Reynolds number, turbulence mixing takes place and because of turbulence the heat transfer coefficient increases.

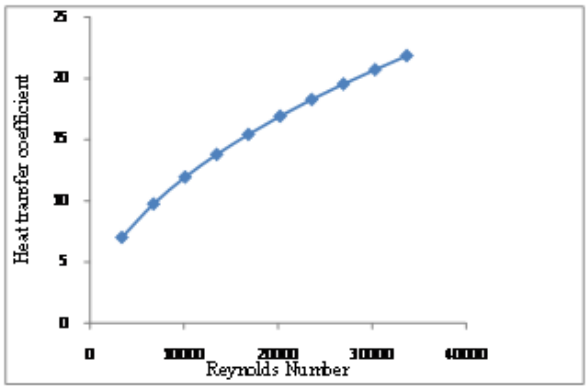

Fig 5. Heat transfer coefficient vs Reynolds number

Fig. 6 shows the variation of friction factor with Reynolds number. It can be seen that as the Reynolds number increases the value of friction factor decreases as expected.This may be attributed to the fact that increases in Reynolds number increases turbulence and decreases friction in the flow.

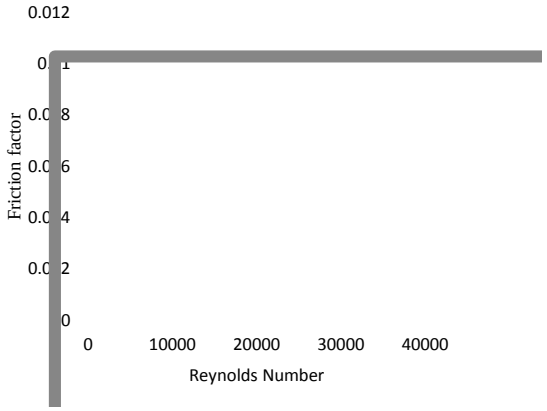

Figure 6. Friction factor vs. Reynolds number

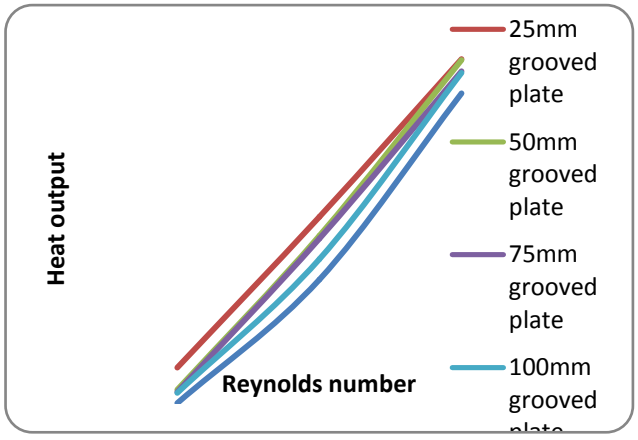

Figure 7. Friction factor vs. Reynolds number

Figure 7 shows variation of heat transfer rate with respect to Reynolds number. It can be seen that heat transfer rate increases as Reynolds number increases as expected. Also it can also be observed that the heat transfer rate is higher for a plate having 25 mm length groove and it decreases as groove length increases. Finally, it can be concluded that grooved plate's helps in better enhancing the heat transfer rate compared to flat plates without grooves.

4. Conclusions

The present study deals with the heat transfer characteristics of plates with rectangular grooves placed vertically within horizontally confining walls. The steady state laminar flow forced convection heat transfer analysis of plate with rectangular groove having different length to depth ratio was undertaken. The discharge and heat flux was varied in this experiment and the following conclusions were drawn

1. Length to width ratio has major impact on heat transfer characteristics.
2. With increasing length to depth ratio of grooves the Nusselt number decreases.
3. With increase in Reynolds number, the coefficient of friction decreases but the rate in decrease is very low as Reynolds number increases.
4. The Nusselt number and heat transfer coefficient increases with increase in the flow rate.
5. Among other plates, the plate of 25mm groove length has highest heat transfer rate.

REFERENCES

[1] Ashish Dixita & Anil Kumar Patila' Heat Transfer Characteristics of Grooved Fin under Forced Convection' Heat Transfer Engineering, vol 36:16, pp.1409-1416, 2015

[2] Chang, S. W., Su, L. M., Yang, T. L., and Chiou, S. F., Enhanced Heat Transfer of Forced Convective Fin Flow With Transverse Ribs, International Journal of Thermal Science, vol. 43, pp. 185–200, 2004.

[3] Kadir Bilen , Murat Cetin , Hasan Gul , Tuba Balta ' The investigation of groove geometry effect on heat transfer for internally grooved tubes, Applied Thermal Engineering, vol. 29 pp.753-761, 2009.

[4] Faheem Akthar, Abdul Razak R Kaladgi and Mohammed Samee A Dafedar, Heat transfer enhancement using dimple surfaces under natural convection—an experimental study, Int. J. Mech. Eng. & Rob. Res. Vol. 4, No. 1, 2015.

[5] Amjad Khan, Mohammed Zakir Bellary, Mohammad Ziaullah, Abdul Razak Kaladgi, An Experimental Approach to Determine the Effect of Different Orientation of Dimples on Flat Plates, American Journal of Electrical Power and Energy Systems, vol.4, pp. 29-33, 2015.

[6]] N. K. Ghaddar, K.Z. Korczak, B.B. Mikic, A.Y. Patera, Numerical investigation of incompressible flow in grooved channels. Part 1. Stability and self-sustained oscillations, J. Fluid Mech. Vol-163 pp.99–127, 1986.

[7] TANG Xinyi and ZHU Dongsheng 'Experimental and Numerical Study on Heat Transfer Enhancement of a Rectangular Channel with Discontinuous Crossed Ribs and Grooves' Chinese Journal of Chemical Engineering, Vol 20, pp.220-230 ,2012.

TRANSIENT HEAT TRANSFER ANALYSIS OF DIMPLED ROD

Abdul Rajak Kaldgi[1*], Abdul Rajak Buradi[2], Vishwanath K C[3], N. Sreenivasalu Reddy[3], Rayid Muneer[1], Mohammed Avvad[1], Chandrasekhar A[4], Asif Afzal[1] and Ahamed Saleel C[5*]

[1]P. A. College of Engineering (Affiliated to Visvesvaraya Technological University), Mangalore, India

[2]NITTE Meenakshi Institute of Technology (NMIT), Bangalore

[3]Raja Rajeswari College of Engineering, Bangalore, India

[4] Bangalore Institute of technology, Bangalore, India

[5]Department of Mechanical Engineering, College of Engineering, King Khalid University, Abha, Saudi Arabia

Corresponding author: ahamedsaleel@gmail.com, arkmech9@gmail.com

Abstract. The considerable heat transfer increase that the dimple causes has led to an interest in its technology recently, with pressure drop penalties lesser than other heat augmentation types. The increase in heat transfer using dimples is based on the fact that the scrubbing of cooling fluid occurs within the dimple and intensifies the delay of flow separation over the surface. The researchers have used different dimple-shaped geometries from all the research studied, such as triangular, ellipsoidal, circular, square, from which the ellipsoidal shape offers better results than other shapes because of prior vortex development. The present work mainly aims to study the dimpled specimen's transient properties and determine their influence on heat transfer.

1. INTRODUCTION

In several fields of application, such as microelectronic cooling, gas turbine internal airfoil cooling, nuclear power plant fuel components, and biomedical equipment, there is a relentless attempt to find ways to increase heat transfer. Two methods are generally adapted for enhancing the heat transfer: Active techniques and Passive techniques. In passive methods, the heat transfer rate is increased by producing surface modifications such as protrusions, dimples, and pin fins. The dimples (surface indentations) are considered necessary because the material is significantly reduced in dimple production, while excessive material is used in pin-fin or rib tabulators, which increases the equipment's weight and cost. A variety of Computational and experimental work has been carried out to enhance the transfer of heat. In 1971, the first person to try using dimples on the surface for heat transfer enhancement was Kuethe[1]. According to him, the dimples would help promote vortexes' creation, resulting in heat transfer improvement [1]. V.N Afnasyev[2] performed an experimental analysis on surfaces formed by spherical cavity networks and observed that, relative to the plane surface, heat transfer improved by 150 percent. Nikolai Kornev[3] investigated vortex structure and heat transfer enhancement in turbulent flow over the staggered dimple array in the narrow channel

using Large Eddy Simulation. The impact of the dimple aspect ratio, temperature ratio, Reynolds number, and flow structure in the dimple channel was studied by Mahmood and Ligrani [4]. A numerical simulation of laminar channel flow over the dimpled surface was conducted by Wang [5], and within a single dimple, an asymmetric 3D horseshoe vortex was found. Experimental research was performed by S.L.Borse and I.H Patel[6] on the influence of dimples on heat transfer under forced convection over a flat surface. They claimed that surface dimples contributed to a lower pressure drop in heat transfer enhancement and indicated that heat transfer enhancement in staggered arrangements is more efficient than inline arrangements. The channel height effect on the heat flow over the dimpled surfaces was studied by Moon [7].

The heat transfer coefficient and friction factors were computationally explored in rectangular channels with dimples on one wall. Pisal and Ranaware[8] have experimented to determine whether dimples on a heat sink fin can enhance heat transfer for laminar airflow. It was carried out using two distinct types of circular dimples (spherical) and oval dimples (elliptical). These dimples were located on both sides of the copper plate; it had a relative pitch of S/D=1.20, and a relative depth of δ/D=0.2. The Nusselt number and overall heat transfer coefficient are calculated for these configurations. Between the 600 and 2000 scale, heat transfer improvements were observed. Katkhaw et al. [9] analyzed the flat surface with an outer flow ellipsoidal dimple with ten types of different arrangements and dimple intervals. For such a dimpled surface, the heat transfer was measured and contrasted with a smooth surface's heat transfer. Results revealed that for staggered arrangement, the heat transfer coefficients were 15.8% more than that for a smooth surface and 21.7% more for inline arrangement. By the transient wide band liquid crystal process, an eight-by-eight jet array will affect a staggering array of dimples at Reynolds number 11,500 as investigated by Kanokjaruvijit Martinez-Botas[10]. Two dimple geometries were tested for hemispherical and cusped elliptical shapes. The study of dimple geometry's effect showed that hemispherical and cusped elliptical dimples did not behave differently significantly. However, compared to the economy, production, and loss of pressure, the hemispheric type should be preferred. Various similar studies can be found in [11-29].

From the literature, it is clear that dimples play a significant role in heat transfer enhancement. However, the unsteady heat transfer analysis for different dimple orientation and material is scarce; this is the primary motivation behind this paper. The main objectives were to find the cooling curve, rate of convective cooling at any instant, and the total amount of heat transfer at a given time. Additionally, the effect of dimple orientation on the heat transfer rate, the cooling medium's influence on the heat transfer rate, and the heat transfer coefficients for different cooling mediums and different dimple orientations were also discussed.).

2. EXPERIMENTAL METHODOLOGY

2.1. Experimental setup

The apparatus is a large insulated water bath with a volume of approximately 30 liters (Fig 4.1). A 3 kW electric heater powered by a thermostat to achieve a constant bath temperature is at the bath's bottom. A rotary switch located in the front of the bath regulates the water temperature. The water bath cover assembly is designed to allow the test specimen to be quickly placed into the bath while maintaining the flow conditions. The test sample is connected to the carrier assembly, and for uniform heat transfer through the water bath, the water bath is stirred continuously. The thermocouple labeled T1 indicates the brass temperature, and the thermocouple labeled T2 indicates the water bath temperature.

2.2. Preparation of test specimen

Brass is the material considered for testing, and the dimples have been machined with the assistance of CNC end milling on the surface of the material. The dimples were machined with a diameter of 4mm and a total depth of 4mm in which 2mm depth has a cylindrical profile, and the remaining 2mm has a concave profile. Two types of orientation were considered to study the influence of dimple orientation on the transient properties, which are inline configuration and circumferentially Staggered orientation. The inline configuration has the dimples located at 90° apart with a spacing of 10cm along the length

(as shown in Fig 2). Circumferentially staggered orientation has the dimples located 90° apart but are provided with an offset along each corner's length (Fig 4.3).

Fig 1 Unsteady state test rig

Fig 2. Inline configuration

Fig 3. Circumferentially Staggered

3. RESULTS AND DISCUSSION

The study presents the experimental results of a cylindrical brass specimen with dimples machined with two configurations: 1) Inline configuration and 2) Circumferentially staggered configuration. The study presents the cooling curve, rate of convective cooling at any instant of time, the total amount of heat transfer at a given time. It also provides the effect of dimple orientation on the heat transfer rate, the cooling medium's influence on the heat transfer rate, and the heat transfer coefficients for different cooling mediums and different dimple orientation.

The following graph (Fig. 4(a)and 4(b)) illustrates the decay rate in temperature and heat transfer coefficient with time. The decay rate is higher in the dimpled rod than the ordinary rod in air cooling. We can also notice that the better results are obtained for inline when compared to the random arrangement.

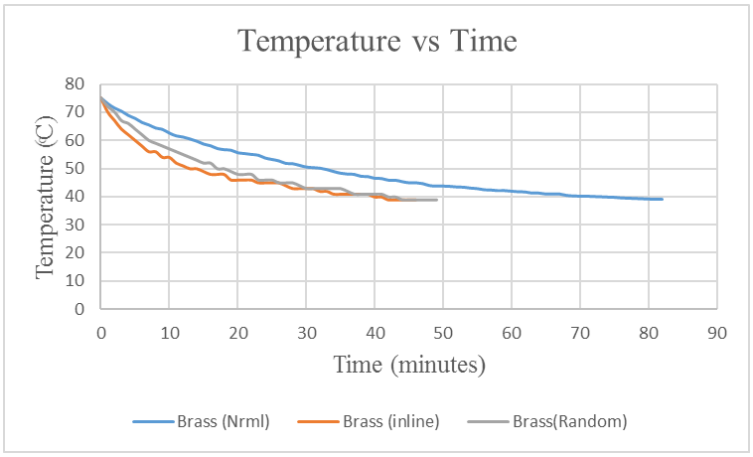

Fig 4 a Temperature vs. Time plot for Brass with air cooling

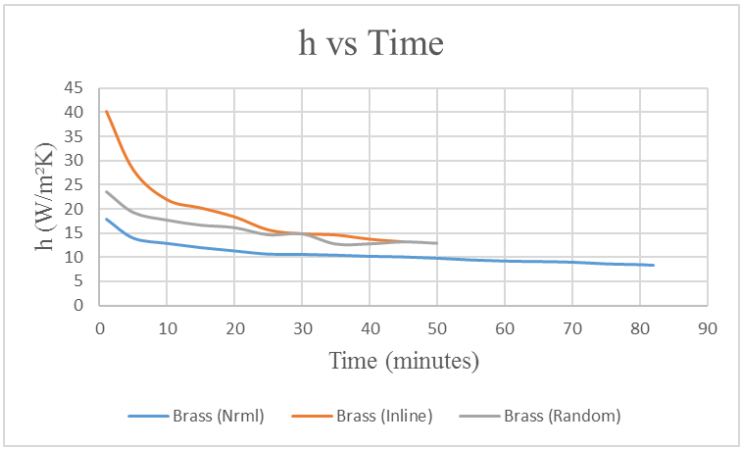

Fig 4 b. Heat transfer coefficient vs. Time plot for Brass with air cooling

Figures 5(a) and 5(b) illustrate the change in temperature and heat transfer coefficient when the cooling medium is water. It can be seen that the decay in temperature is almost the same for both the dimpled orientations. However, significant heat transfer enhancement can be seen in the dimpled surface compared to the ordinary rod.

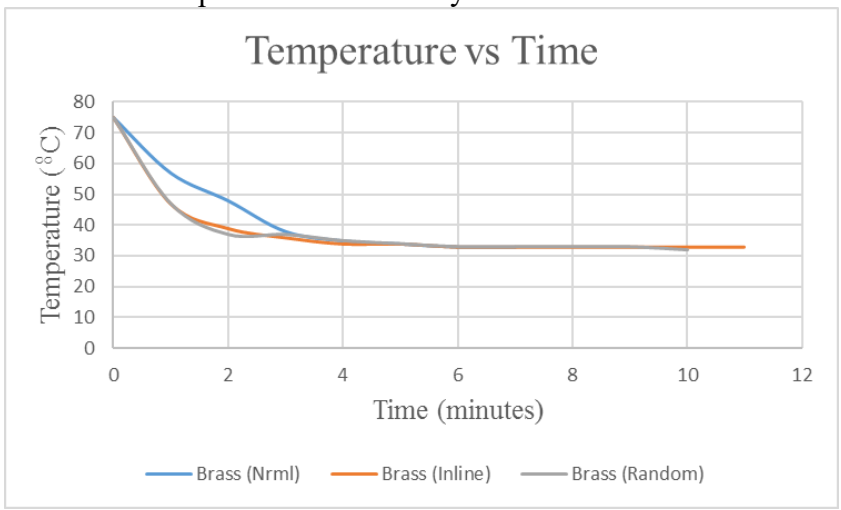

Figure 5 a. Temperature vs. Time plot for Brass with water cooling

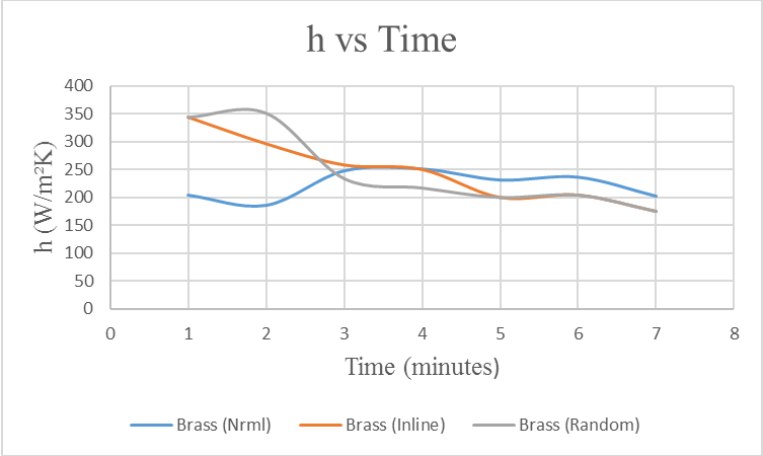

Figure 5 b Heat transfer coefficient vs. Time plot for Brass with water cooling

The following graph (Fig. 6(a) and 6(b)) shows the variation of temperature and heat transfer coefficient with time for a radiator coolant. It illustrates that there was no significant heat transfer enhancement when the cooling medium was a radiator coolant. It is because of the reason that a coolant circulation system is required to remove heat effectively.

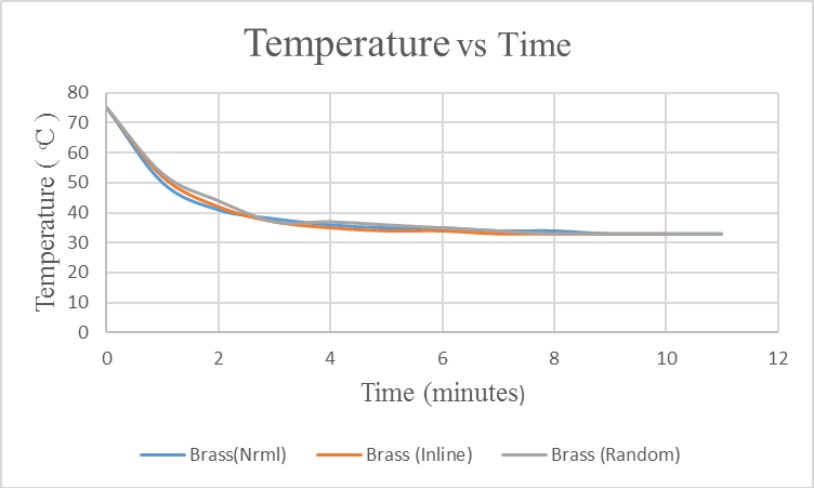

Fig 6 a Temperature vs. Time plot for Brass with coolant cooling

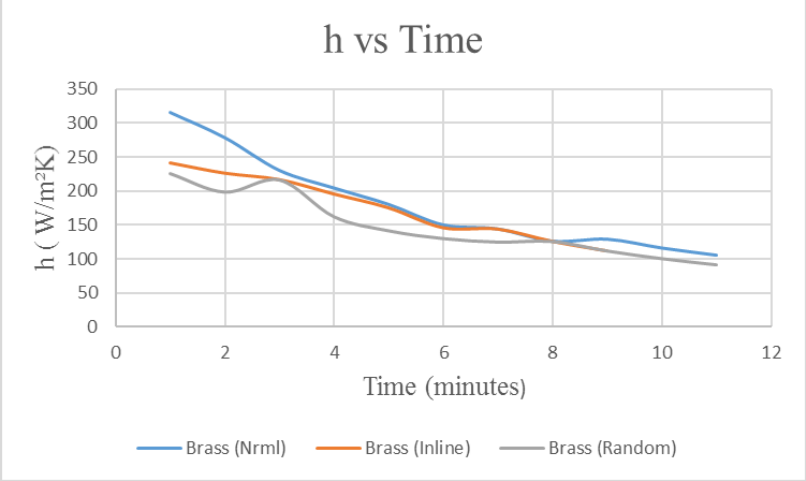

Fig 6 b Heat transfer coefficient vs. Time plot for Brass with coolant cooling

4. CONCLUSIONS

From the results obtained, we can conclude that there was considerable heat transfer enhancement with dimples' introduction. Heat transfer enhancement concerning dimples' inline configuration was more than the staggered arrangement of dimples. The convective cooling and total heat transfer rate also increased after the introduction of dimples for air cooling. When the cooling medium was water, there was no distinction between the heat transfer from specimens with inline and staggered configuration. Surprisingly, when a coolant was used, there was probably no heat transfer enhancement seen.

References

[1] Kuethe A. M., Boundary Layer Control of Flow Separation and Heat Exchange. US Patent No. 1191,1970.
[2] Afanasyev, V.N., Chudnovsky, Y.P., Leontiev, A.I., and Roganov, P.S, Turbulent flow friction and heat transfer characteristics for spherical cavities on a flat plate. Experimental Thermal Fluid Science, Vol.7, Issue 1, pp. 1–8, 1993.
[3] Chyu, M.K., Yu, Y., Ding, H., Downs, J.P., and Soechting, F.O., Concavity enhanced heat transfer in an internal cooling passage In Orlando international Gs Turbine & Aero engine Congress & Exhibition, Proceedings of the 1997(ASME paper 97-GT-437), 1997.
[4] Mahmood, G.I., Hill, M.L., Nelson, D.L., Ligrani, P.M., Moon, H.K. and Glezer.B., Local heat transfer and flow structure on and above a dimpled surface in a channel. J Turbomach, Vol.123, Issue 1, pp: 115–23, 2001.
[5] Dewan, A., Mahanta, P., Raju,K.S., and Kumar.P.S.,Review of passive heat transfer augmentation techniques. Proc. Instn Mech. Engrs, Part A: J. Power and Energy, Vol. 218, pp. 509–527, 2004.
[6] Liu S, and Sakr ,M.A., comprehensive review on passive heat transfer enhancements in pipe exchangers. Renewable and Sustainable Energy Reviews, Vol.19 pp. 64–81, 2013.
[7] Hasibur Rahman Sardar, Abdul Razak Kaladgi. Forced Convection Heat Transfer Analysis through Dimpled Surfaces with Different Arrangements. American Journal of Energy Engineering. Vol. 3, No. 3, 2015, pp. 37-45.
[8] Hasibur Rahman Sardar, Abdul Razak Kaladgi. Forced Convection Heat Transfer Analysis through Dimpled Surfaces with Different Arrangements. American Journal of Energy Engineering. Vol. 3, No. 3, 2015, pp. 37-45.
[9] Katkhaw, N., Vorayos, N., Kiatsiriroat, T., Khunatorn, Y., Bunturat, D. and Nuntaphan, A., 2014. Heat transfer behavior of flat plate having 45 ellipsoidal dimpled surfaces. Case Studies in Thermal Engineering, 2, pp.67-74.
[10] Kanokjaruvijit, K. and Martinez-botas, R.F., 2005. Jet impingement on a dimpled surface with different crossflow schemes. International journal of heat and mass transfer, 48(1), pp.161-170.
[11] Afzal A, Mohammed Samee AD, Abdul Razak RK, Ramis MK. Thermal management of modern electric vehicle battery systems (MEVBS). Journal of Thermal Analysis and Calorimetry. 2020 Apr 3:1-5.
[12] Afzal, A., Mohammed Samee, A. M., Razak, R. A., & Ramis, M. K. (2019). Effect of spacing on thermal performance characteristics of Li-ion battery cells. Journal of Thermal Analysis and Calorimetry, 135(3), 1797-1811.
[13] Razak RA, Afzal A, Samee AM, Ramis MK. ‘’Effect of cladding on thermal behaviour of nuclear fuel element with non-uniform heat generation’’. Progress in Nuclear Energy. 2019 Mar 1; 111:1-14.
[14] Afzal A, Samee AM, Razak RA, Ramis MK. ‘Steady and Transient State Analyses on Conjugate Laminar Forced Convection Heat Transfer’’. Archives of Computational Methods in Engineering (Springer, Impact factor: 7.605). ISSN: 1134-3060,

Characterization of Ballistic and Wear Resistance of Friction Stir Welded AA6061 Aluminium Alloy

K C Vishwanath[1], N. Sreenivasalu Reddy[1], A Chandrashekar[2]

[1]*Department of Mechanical Engineering, Raja Rajeswari College of Engineering Bangalore, Karnataka, INDIA*
[2]*Department. of Mechanical Engineering, Bangalore Institute of Technology, Bangalore, Karnataka, INDIA*

Corresponding Author: [a)]vishwa8160@gmail.com; [b)]acsmech@gmail.com

ABSTRACT

The aim of the research work was to investigate on the Friction stir welding (FSW) process which is particularly suitable for welding aluminium produces higher quality welds with material properties closer to the parent metal as compared to most other welding processes. A non-consumable tool is used to generate frictional heat in the abutting surfaces. A shoulder and a pin are the important parts of the tool. This tool makes weld without conventional defects with good mechanical properties and is especially suited for aerospace, defence and marine applications. In addition, because friction stir welding is performed below the melting temperature, protection requirements are greatly reduced. These reasons make this welding process suitable for many applications in aerospace industries. In the present study, FSW process is carried out on aluminium alloy AA6061 plates by varying process parameters such as weld speed (WS) and tool rotational speed (TRS) using cylindrical pin profiled tool. These process parameters are optimized by using the Design of Experiments (DOE) approach. Tests for tribological and ballistic characteristics are conducted on the welds. Under considered set of experimentation, the friction stir welded AA 6061 alloy showed its best for tool rotation speed 900 rpm and traverse speed of 30 mm/min for straight cylindrical pin configuration in comparison with rest of the combinations considered in the study. This optimized combination yielded with reduced wear rate (1.0811×10^{-3} mm^3/N-m) and resistance to ballistic impact.

Keywords: Ballistic Resistance; Wear Resistance; Aluminium Alloy; Friction Stir Welding

INTRODUCTION

Aluminium, the second most plentiful metallic element on earth, became an economic competitor in engineering applications as recently as the end of the 19th century. The emergence of three important industrial developments would, by demanding material characteristics consistent with the unique qualities of aluminium and its alloys, greatly benefit growth in the production and use of the new metal. Electrification would require immense quantities of light-weight conductive metal for long-distance transmission and for construction of the towers needed to support the overhead network of cables which deliver electrical energy from sites of power generation. Aluminium industry works for the structurally reliable, strong, and fracture-resistant parts for airframes, engines, and ultimately, for missile bodies, fuel cells, and satellite components. The properties of aluminium that make this metal and its alloys the most economical and attractive for a wide variety of uses are its appearance, light weight, fabric ability, physical properties, mechanical properties and corrosion resistance [1]. Aluminium has a density of only 2.7 g/cm^3, approximately one-third as much as steel (7.83 g/cm^3), copper (8.93 g/cm^3), or brass (8.53 g/cm^3).

Proceedings of International Conference on Advances in Materials Research (ICAMR - 2019)
AIP Conf. Proc. 2274, 030050-1–030050-8; https://doi.org/10.1063/5.0022418
Published by AIP Publishing. 978-0-7354-4004-3/$30.00

It can display excellent corrosion resistance in most environments, including atmosphere, water (including salt water), petrochemicals, and many chemical systems. Aluminium typically displays excellent electrical and thermal conductivity, but specific alloys have been developed with high degrees of electrical resistivity. These alloys are useful, for example, in high-torque electric motors. Aluminium is often selected for its electrical conductivity, which is nearly twice that of copper on an equivalent weight basis. Aluminium is non ferromagnetic, a property of importance in the electrical and electronics industries. Aluminium is also nontoxic and is routinely used in containers for foods and beverages. Some aluminium alloys exceed structural steel in strength. However, pure aluminium and certain aluminium alloys are noted for extremely low strength and hardness.

Fusion welding processes like gas metal arc welding, gas tungsten arc welding, resistance welding, stud arc welding can be used for welding most of the aluminum alloys [2]. When arc welding process is used, distortion control, prevention of shrinkage voids and control of crater cracking are necessary. Specific properties that affect aluminum welding are its oxide characteristics, the solubility of hydrogen in molten aluminum, its thermal, electrical and nonmagnetic characteristics, its lack of colour change when heated and its wide range of mechanical properties and melting temperatures that result from alloying with other metals. Problems like porosity, lack of fusion due to oxide layers, incomplete penetration, cracks, inclusions and undercut occur when welding aluminum alloys. The strong chemical affinity of aluminum to oxygen results in the formation of aluminum oxides with melting point higher than that of the alloy. During fusion welding, the presence of aluminum oxides results in incomplete fusion, and if the oxide is thick, arc initiation is prevented. Chemical or mechanical cleaning is needed for removing these oxides. Special methods such as inert gas welding, or use of fluxes is necessary if aluminum has to be welded using the fusion welding processes. The solubility of hydrogen in liquid aluminum is very high while hydrogen has almost no solubility in solid aluminum at room temperature. When the weld pool is at high temperature and the metal is still in liquid state, it absorbs lots of hydrogen. When the weld solidifies, hydrogen which did not escape is trapped and forms gas porosity [3]. This demands considerable cleaning and preparation to eliminate all possible sources of hydrogen. Another major problem during fusion welding of aluminum alloys is hot cracking. The high thermal expansion coefficient, solidification shrinkage and its wide range of solidification temperatures make the alloys highly susceptible to hot cracking during welding of aluminum. Cracking sensitivity of heat treatable alloys is of concern as these alloys have greater amounts of alloying elements [4]. The colour of aluminum remains unchanged during welding; this requires keen attention to follow the weld line which leads to the exposure of the welder to harmful radiations due to high reflectivity of aluminum.

The weldability of some aluminum alloys is an issue with the fusion welding processes. Fusion welding is not suitable for 2xxx series (Al-Cu) of aluminum alloys. The copper content causes hot cracking, poor solidification microstructure and porosity in the fusion zone [5]. The 5xxx series (Al-Mg) of aluminum alloys with more than 3 % of Mg content is susceptible to cracking due to stress concentration in corrosive environments, so high Mg alloys of 5xxx series are generally not exposed to corrosive environments at high temperatures to avoid stress corrosion cracking. The 6xxx series (Al-Mg-Si) aluminum alloys are readily weldable, but sometimes susceptible to hot cracking under certain conditions. The 7xxx series (Al-Mg-Zn) of aluminum alloys have high tendency to hot crack after welding. All the 7xxx series have the sensitivity to stress corrosion cracking. All these problems associated with the welding of different alloys of aluminum have hindered their usage in industrial applications. With development of solid state welding processes like Friction stir welding (FSW), aluminum alloys such as 2xxx, 7xxx and 8xxx series which were difficult to be welded by fusion welding processes have been successfully welded. As friction stir welding process joins material at temperatures below the melting temperature of the base metal, problems occurring in the conventional welding process are eliminated and sound joints are produced even in materials that were extremely difficult to weld using conventional fusion welding processes [6]. Because of its advantages, the process finds many applications like ship building, marine industries, aerospace industries, automotive industries and railway industries. Although the process was initially used for welding aluminum alloys, homogenous and heterogeneous welding of brass, copper, lead, magnesium, carbon steel, stainless steel, titanium, and other alloys have been explored and seem to be successful. The mechanism of FSW, resulting microstructure, mechanical properties, corrosion, fatigue and fracture behavior of the joints have been areas of constant research over the past few years.

MATERIALS AND EXPERIMENTAL METHOD

Friction Stir welding (FSW), is a solid state joining process invented and patented in Great Britain at 'The Welding Institute' (TWI), during 1990's. Since its invention, the process has received world-wide attention, and today FSW is used in research and production in many sectors, including aerospace, automotive, railway, shipbuilding, electronic housings, coolers, heat exchangers, and nuclear waste containers. FSW has been proven to be an effective process for welding aluminum, brass, copper, and other low-melting-temperature materials. The latest phase in FSW research has been aimed at expanding the usefulness of this procedure in high-melting-temperature materials, such as carbon and stainless steels and nickel-based alloys, by developing tools that can withstand the high temperatures and pressures needed to effectively join these materials.

During friction stir welding, most of the heat is generated as a result of material deformation due to the tool rotation effect. The peak temperature within the weld region is dependent on the used tool size, shape, rotation and traverse speed.. The larger the tool diameter, the higher the rotation speed and the lower traverse speed, the higher the heat input is expected. On the contrary, the higher traverse speed and or lower rotating speed, then the lower the heat input within the weld is generated. This might not be sufficient to soften the material, resulting in improper material flow, pin damage, and formation of defects as shown in Fig.1.

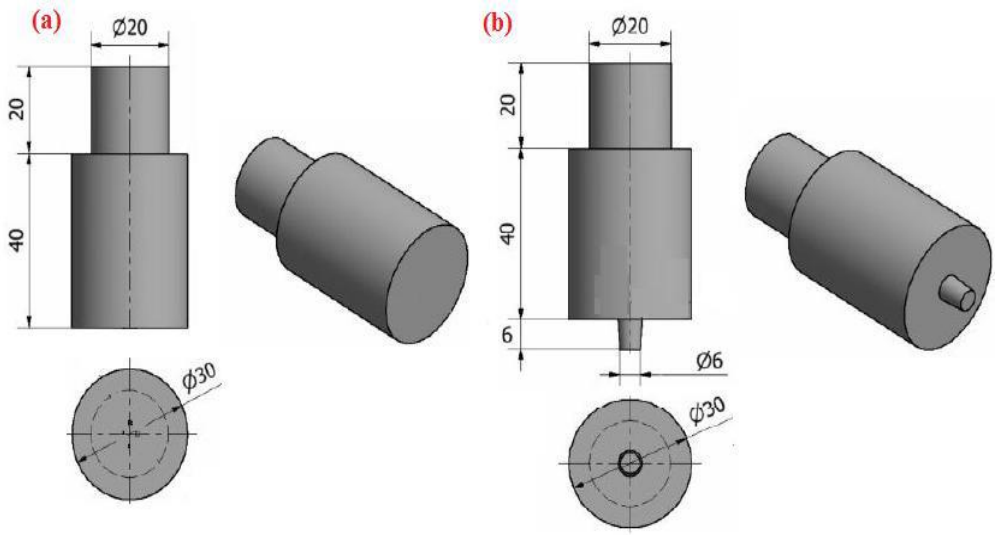

FIGURE 1. Tools used in the study (a) Pin less FSP tool (b) FSW tool with cylindrical pin profile

The mechanical and corrosion properties of the joined components are highly affected by the amount of the heat induced during joining. Extra heat leads to reduced mechanical and corrosion properties. Minimizing the heat input will possibly reduce such risk. Ideally, the temperature should not be reduced to an extent that the material softening underneath the probe will not take place. For this reason, proper welding parameters have to be selected to insure that the temperature around the tool is sufficiently high to provide an adequate material flow Fig.2. The heat generated from the process modifies the post welded microstructure and creates distinct regions with different microstructures.

(a)

(b)

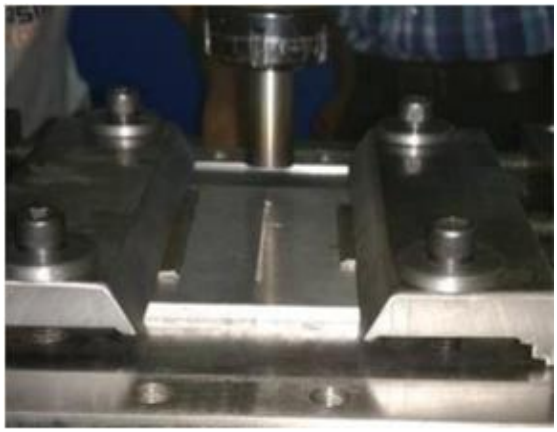

(c)

(d)

(e)

f)

FIGURE 2. Different stages of the FSW (a) Pistachio powder, (b) Specimen having groove, fixed on the work table, (c) Work pieces are set on the table, Tool drives over the surface, (d) Temperature Measuring During Process Using Infrared Thermometer, (e) Transverse feed given along with speed, f) Completed Joint Rotational

Ballistic Test

Ballistics is a field in mechanics that deals with the study of the launching, flight behavior and effects of the projectile on the target. Earliest known projectiles were arrows, stones or splints that may or may not have been propelled by a bow or a catapult. It is also deals with the design in the projectile and its acceleration in order to achieve the desired performance Fig. 3. The real time Ballistic testing generally deals with the dimensions of the bullets, then distance of the specimen from where the firing gun is placed, and type of specimen which should withstand the Bullets impact load. The ballistic testing is basically followed by ASTM Ballistic standards Fig. 4.

Brief History is as follows:

- 1493-1508- Emperor Maximilian of Germany proposed rifling of guns in order to impart rotatory motion to the projectile during firing.
- 1835- Henry Goddard of the Bow Street Runners examined the bullet from the crime scene and noticed a defect on it.

1860- In the Regina vs. Richardson case the evidence included newspaper wadding used to seal the bullet from the gunpowder. The wadding was found on the victims wounds which contained The London Times paper of March 27th 1854.

- 1902- Oliver Wendell Holmes turned to magnification on account of increased firearms manufacture which lead to standardization of rifling.
- 1912- Professor Balthazar used photography to document circumferences of the bullets found at the crime scenes and those test fired.
- 1925- Charles E. Waite along with Calvin Goddard, Philippe Gravelle and John Fischer founded the Bureau Forensic Ballistics in New York. Gravelle developed comparison microscope and Fischer invented the helixometer.

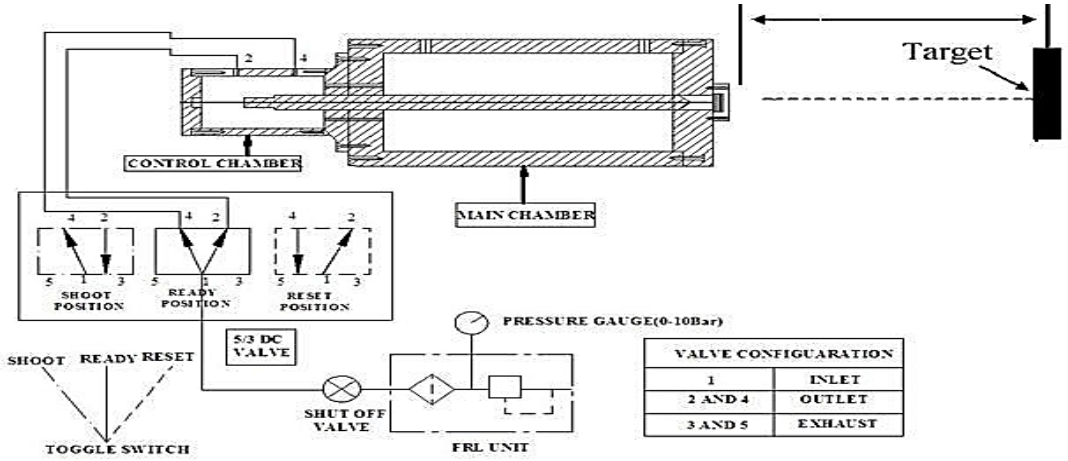

FIGURE 3. Schematic of Ballistic Impact test

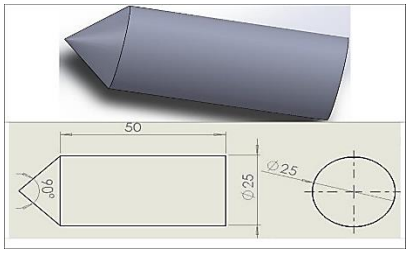

FIGURE 4. Pictorial view and dimensions of the bullet used in ballistic study

Pin-on-disc wear testing machine Fig.5 (Make: DUCOM Instruments Pvt. Ltd., Bengaluru, Model: TR20-LE), shown in Fig, was used to measure the wear characteristics of the specimens as per ASTM-G99-95 standards. Wear test conditions chosen for conducting experiments on friction stir welds are given in Table.1

Figure 5. 'Pin-on-Disc' wear testing machine

TABLE 1. Wear test parameters used for friction stir welds

Pin material	FSWed AA6061
Contact Pin shape	Square
Disc material	EN32 steel disc - 65 HRC
Pin contact area (mm^2)	36
Specimen Height (mm)	25
Track diameter (mm)	100
Load (N)	14.715
Sliding speed (m/s)	2.660
Temperature	Room temperature
Sliding distance (m)	6000

The specific wear rate (W_s) of the pin was calculated using the following relation

RESULTS AND DISCUSSIONS

Front end appearance of target after ballistic testing is shown in Fig 6. Ballistic testing with lead projectile has resulted in damage, in the form of a perforation hole with measurable depth of penetration, and width of the hole. The ballistic performance was characterized by the depth of penetration of the projectile in the target plate and width of hole. The depth of penetration of damaged targets was measured by microscope. Width of the perforation hole and total crack depth were measured for each target and is presented in Table 2. It gives the comparative data of the ballistic testing of base metal and friction stir welded specimens.

FIGURE 6. Front end appearance of target after ballistic testing

TABLE 2. Diameter and depth of indentation after ballistic test

Sl. No	Rotational Speed, Rpm	Welding Speed, mm/min	Diameter of indentation		Depth of indentation	
			Weld zone (mm)	Heat affected zone (mm)	Weld zone (mm)	Heat affected zone (mm)
1	900	50	2.5391	2.2650	0.7933	0.7103
2	700	30	2.6244	2.5121	0.8059	0.7987
3	800	40	2.7376	2.5321	0.9419	0.8564
4	700	50	2.6589	2.5590	0.4208	0.6746
5	800	50	2.3811	1.7035	0.7179	0.4990
6	800	30	2.6489	1.9781	0.6200	0.2573
7	900	40	2.6497	2.4001	0.7522	0.6735
8	700	40	2.5880	2.3739	0.4701	0.3991
9	900	30	2.5725	2.2726	0.6634	0.3132

Table 3 Specific wear rate for different welded joints

Sl. No	Rotational Speed, Rpm	Welding Speed, mm/min	Initial weight $w_1$gms	Initial weight $w_2$gms	Specific wear rate $*10^{-3}$ mm^3/N-m		Error %
					Expt.	Predicted	
1	900	50	3.7674	3.3290	1.8301	1.77780	2.94
2	700	30	3.8181	3.7083	4.5900	4.53773	1.15
3	800	40	3.7797	3.4033	1.5788	1.52653	3.42
4	700	50	3.6617	3.2369	1.7800	1.65027	7.86
5	800	50	3.6907	3.2844	1.7030	1.88500	-9.65
6	800	30	3.4948	3.0988	1.6601	1.53037	8.47
7	900	40	3.8447	3.4211	4.7912	4.66140	2.78
8	700	40	3.8150	3.4163	4.5120	4.69400	-3.87
9	900	30	3.8145	3.5563	1.0811	1.26310	-14.40

Scanning Electron Microscopy (SEM)

Fig. 7 shows the SEM micrographs of worn surface for welded plate number 9 fabricated under tool rotational speed of 800 rpm and traverse speed of 50 mm/min using straight cylindrical pin Fig.7. It can be seen that unlike other welded plates, it consisted large parallel groove with a little delamination seen in the wear track.

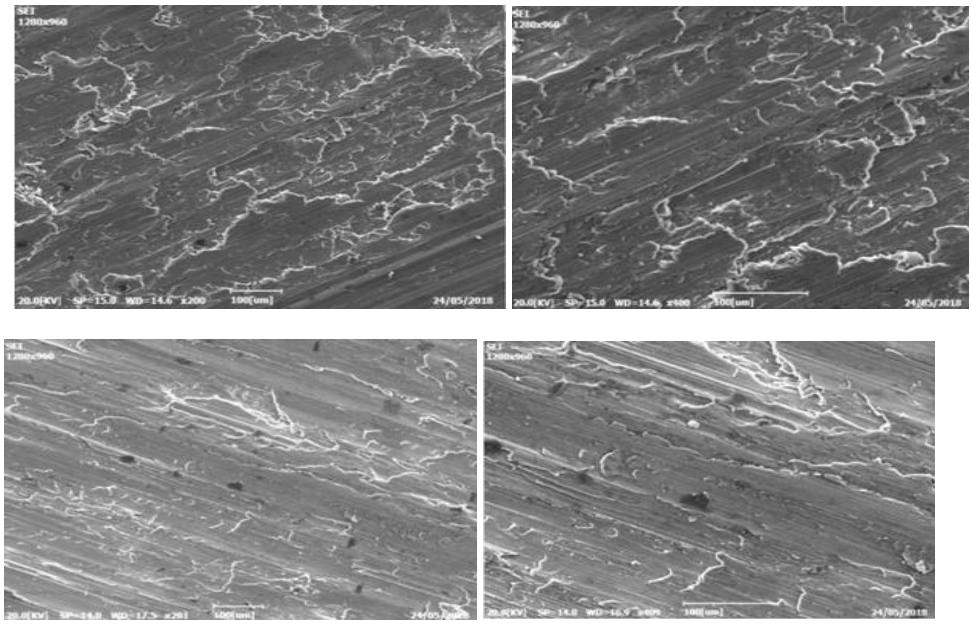

FIGURE 7. Worn out surface of a joint welded with (a) 900 rpm, 50 mm/min and SC tool, (b) 700 rpm, 30 mm/min and SC tool

CONCLUSIONS

In the present work, AA 6061 plates having 6 mm thick were successfully welded using friction stir welding technique for different process parameters such as rotational speed (viz. 700, 800 and 900 rpm) and welding speed (viz. 30, 40 and 50 mm/min) using cylindrical profiled pin tool. For all the fabricated joints based on design matrix, the tribological and ballistic properties were evaluated and discussed in detail. In friction stir welded AA 6061 alloy, process parameters (rotation speed and traverse speed) and tool configuration have proved their role in influencing the properties of the welded joints. The case of friction stir welded AA 6061 alloy, tool rotation speed 900 rpm, traverse speed of 30 mm/min and straight cylindrical pin configuration shows better properties. Comparison with rest of the combinations considered, this optimized combination yielded with reduced wear rate (1.0811×10^{-3} mm^3/N-m).

REFERENCES

1. S. K. Tiwari, Dinesh Kumar Shukla and R. Chandra, International Journal of Mechanical, Aerospace, Industrial and Mechatronics Engineering, 7 (12), 1343-1346 (2013).
2. Ying Chun Chen, Huijie Liu and JicaiFeng, Mater Science Engineering, A, 420, 21–25 (2006).
3. Sutton M, Yang B, Reynolds A, Taylor R, Materials Science and Engineering, A 323(1-2), 160-166, (2002).
4. Lee Won Bae, Yeon Y M, Jung SB, Effect of friction welding parameters on mechanical and metallurgical properties of aluminum alloy 5052–A36 steel joint, Material Science Technology, 19 (6), 773-778 (2013).
5. Min-Su Han, Seung-Jun Lee, Jae-Cheul Park, Seok-CheolKo, Yong-Bin Woo and Seong-Jong Kim, Transaction of Non Ferrous Society of China, 32, 17-22 (2009).
6. Yan-hua Zhao T, San-bao Lin, Lin Wu and Fu-xingQu, Materials Letters, 59, 2948-2952 (2005).

International Research Journal of Engineering and Technology (IRJET) e-ISSN: 2395-0056
Volume: 06 Issue: 05 | May 2019 www.irjet.net p-ISSN: 2395-0072

EXPERIMENTAL STUDY OF HEAT TRANSFER ON RECEIVER TUBE OF PARABOLIC COLLECTOR WITH CONTINUOUS HELICAL FINS

[1]Kavya S, [1]Ranjitha M, [2]N Srinivasalu Reddy, [3]Vaibhavi D

[1,3]ME Scholar, Department of Mechanical Engineering, Bangalore University, Bangalore, Karnataka, India 560001

[2]Associate Professor, Department of Mechanical Engineering, Raja Rajeswari college of Engineering, Bangalore, Karnataka, India 560074

ABSTRACT:- *Heat transfer is the process of transfer of heat from high temperature reservoir to low temperature reservoir. In terms of the thermodynamic system, heat transfer is the movement of heat across the boundary of the system due to temperature difference between the system and the surroundings. The heat transfer can also take place within the system due to temperature difference at various points inside the system. The difference in temperature is considered to be 'potential' that causes the flow of heat and the heat itself is called as flux. The present work deals with modification of traditional concentric trough collector, receiver tube. Experiments are conducted on a modified receiver tube for various mass flow rates, and different helical pitches. The results reveal that the modified receiver tube of a solar trough collector gives plan move enhancement of heat transfer comparing to receiver tube. The work will be helpful for scientists focusing on sun powered vitality utilizing illustrative.*

Key words*: Single tube; Heat exchanger; Parabolic trough collector; Helical fins*

1. INTRODUCTION

A heat exchanger is a device used to transfer heat between two or more fluids. Heat exchangers are used in both cooling and heating processes. A solar collector is a gadget utilized for gathering solar radiation and exchanges vitality to liquid going in contact with it. Usage of solar vitality requires solar collector. These are general of two types i.e., Concentric and Non concentric type. The solar collector with its related absorber tube is the fundamental segment of any system for the change of solar radiation vitality into more usable shapes e.g. heat or power. In the non concentrating type the gatherer region is same as the absorber zone. Then again concentrating gatherers the zone capturing the solar radiation is more prominent, here and there 100 times more noteworthy than the absorber zone.

Non concentrating: As the name recommends the sun powered radiation is not moved in this compose 1.1 flat plate type solar collector – the principle segments of a flat plate solar are absorber tube, tubes or fins, coating, thermal insulation, cover strips, container or casing. Flat plate solar collector are ordered into 2 kinds, water type collectors which utilize water as the heat exchange liquid and air type collectors which utilize air as the heat exchange liquid. Concentrating: This sort of solar thermal innovation includes convergence of the vitality shape of the sun to a solitary line or focuses. The parabolic trough solar collector utilizes a reflector in the state of a parabola which is for the most part reflect, or an anodized aluminum sheet contingent upon the expected applications to reflect and think the solar radiation towards a beneficiary tube situated at the concentration line of the parabola. The absorber tube might be made of mellow steel or copper an is covered with a warmth safe dark paint for the better execution. The collector ingests the approaching radiations and changes them into warm vitality, which is being transported and gathered by a liquid medium circling inside the recipient tube. The warmth exchange liquid moves through the absorber tube, gets warmed and in this manner conveys thermal. The temperature of the liquid reaches up to 400 degree Celsius. Depending on the warmth exchange prerequisite diverse warmth exchange liquids might be utilized. The experimental data fit well with the numerical for the large heat exchanger. But, there were the some differences between the numerical and experimental data for the smaller coil; however these differences may have been due to the nature of the Wilson plots [11]. Studied the fluid flow and heat transfer characteristics of double type heat exchanger with rotating inner tube. The experiments carried out for the speed of rotation of inner tube from 0 to 1000 rpm. The effectiveness and NTU number obtained for parallel flow and counter flow arrangement. They found that speed of rotation increases the Reynolds numbers, NTU and effectiveness values [12].

2. EXPERIMENTATION

The solar radiations coming parallel to the central line of parabola (reflector) gathers at the surface of reflector and thinks it to the point of convergence. On the off chance that the reflector is as trough with illustrative cross segment, the solar radiation centers along a line. In concentrating collector that a focus proportion is vital parameter.

It is characterized as the proportion of the gather region at which radiation gathers to the territory (absorber) at which these radiations are concentrated. Focus proportion is characterized as the proportion of the authority zone to the absorber zone. So with the lessening in the absorber territory the focus proportion increments and thus more rapidly the high temperatures are come to. So higher fixation proportion implies higher temperature can be accomplished. The schematic outline of the illustrative trough solar authority with the absorber tube, following components and bolster structure.

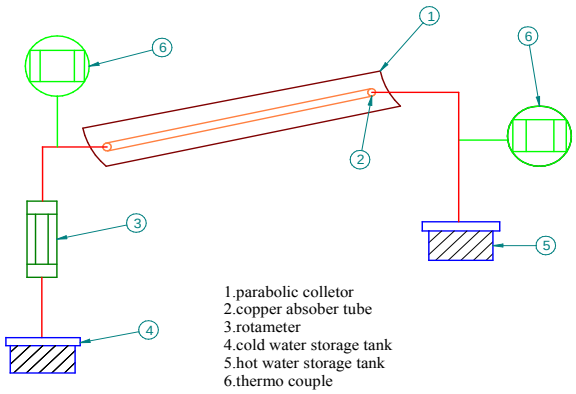

Fig-1: Schematic diagram of experimental setup

A parabolic solar collector uses a reflector in the shape of a parabola which is mostly a mirror, or an anodized Aluminum sheet depending on the required applications to reflect and concentrate the solar radiations towards a receiver tube located at the focus line of the parabola. The absorber tube may be made of mild steel or copper and is coated with a heat resistant black paint for the better performance. The schematic diagram of experimental setup is as shown in Figure 1.

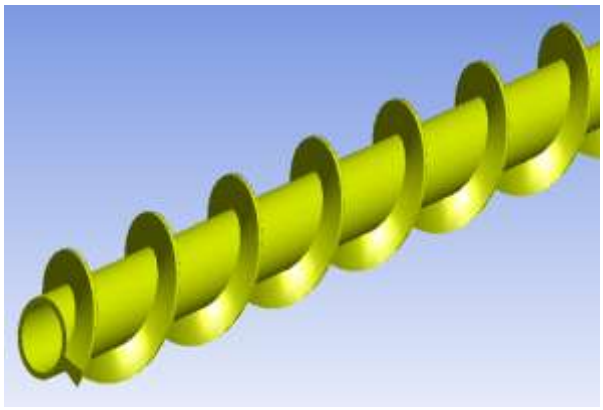

Fig-2: Geometry of helical fins of pitch 50 mm

3. RESULTS AND DISCUSSION

This project discusses the results of rate heat transfer of receiver tube of parabolic trough collector with and without fins for different duration of time. The deliberate factors are flow rate (LPM), temperature of water through temperature test (deg C). The information accumulation has been improved the situation different arrangements of the absorber tube amid 11am-2pm. A few information were dismissed because of high breeze and shady conditions. Results of the heat transfer rate variation of typical helical fin with different fin shown in the figure below combination of the swirling flow rate of the twisted-tape and the generated vortex due to louvered-fins on it.

3.1 Rate of heat transfer at 11-12 noon

Figure 3 shows the variation of rate of heat with volume flow rate for duration of 1 hour from 11-12pm. With reference to Figure 3, it is observed that the rate of heat transfer increases as the volume flow rate increases. The experiments are conducted for three volume flow rates i.e., 0.5LPM, 1LPM and 1.5LPM respectively.

The enhancement of heat transfer is improved in the case of 30mm pitch based annulus and 60mm pitch based annulus as compared to the annulus without fins. The rate of heat transfer for 30mm helical pitch based annulus is more as compared to 60mm helical pitch based annulus. This is due to the surface area of the 30mm helical fin based annulus is more as compared to 60mm helical fin based annulus.

The value rate of heat transfer for 30mm helical pitch, 60mm helical pitch and plain tube are is 1081W,

872.291W, 382.8W res for a volume flow rate of 0.5 liters per minute respectively.

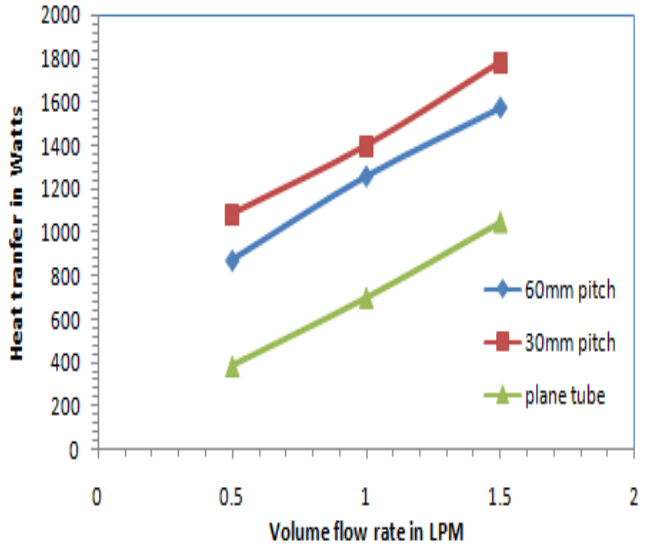

Fig-3: Variation of heat transfer with volume flow rate for the duration of 11-12pm

3.2 Rate of heat transfer at 12-1pm

Figure 4 shows the value rate of heat transfer for 30mm helical pitch, 60mm helical pitch and plain tube are is 1081.6W, 942.075W, 593.1W res for a volume flow rate of 0.5 liters per minute respectively.

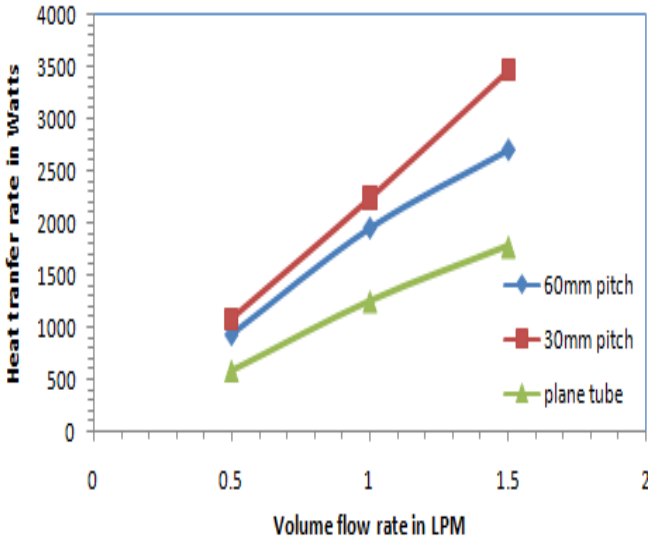

Fig-4 Variation of heat transfer with volume flow rate for the duration of 12-1pm

3.3 Rate of heat transfer at 1-2pm

Figure 5 shows the value rate of heat transfer for 30mm helical pitch, 60mm helical pitch and plain tube are is 558.2W, 453.5W, 383.8W res for a volume flow rate of 0.5 liters per minute respectively.

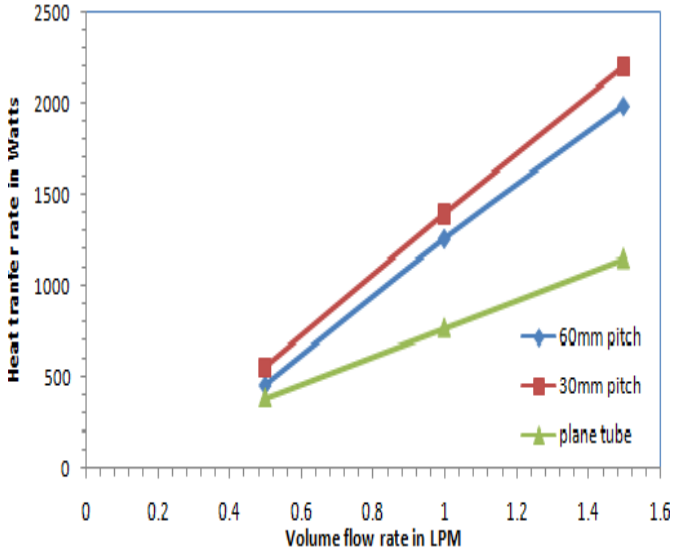

Fig-5 Variation of heat transfer with volume flow rate for the duration of 1-2pm

4. CONCLUSION

In present work the effect of a new continuous helical tape on heat transfer for an absorber tube or solar parabolic trough collector is evaluated experimentally. It is found that higher heat transfer rate is absorbed for 30mm helical pitch based receiver tube as compared to receiver tube without fins. The rate of heat transfer in case of 30mm helical pitch based receiver tube is better as compared to 60mm pitch helical based receiver tube. The application of new continuous helical tape insert resulted high performance especially for low mass flow rate.

REFERENCES

1. Government of india. Ministry of power central electricity authority new delhi, executive summary sector,<http://www.ceaa.nic.in/reports/planning/dmlf/growth> ; february 2014 [accessed 17.07.14]

2. Reddy KS, Ravi kumar K, solar collector field design and viability analysis of stand alone parabolic trough power plants for indian conditions. Energy

3. Sustain dev 2012;16:456-70.\[3] valan arasu A, Sornakumar T. life cycle cost analysis of new FRP based solarparabolic trough collector hot water generation system. J Zhejiang univ sci A2008;9(3):416-22.

4. National renewable energy laboratory (NREL) of the US department of energy. Source from <http://www.nrel.gov/international/ra_India.html>; content last updated: 26th september 2013.

5. Garud shirish, purohit ishan. Making solar thermal power generation in India reality -overview of technologies, opportunities and challenges. India: the energy and resources institute; 2009.

6. Morimoto masato, maruyama toshiro. Static solar concentrator with verticalflat plate photovoltaic cells and switchable white/transparent bottom plate.sol energy master sol cells 2005;87:299-309.

7. Bello-garcia antonio, garcia- cortes silverio, ordonez celestino. Estimatinginterecept factor of a parabolic solar trough collector with new supportingstructure using off the shelfphotogrammetric equipment. Appl energy 2012;92:815-21.

8. EckhardLupfert, michael geyer. Eurotroughdesign issues and prototypetesting at PSA. In: proceedings of solar forum 2001. solar energy, 21-25april;2001.

9. Vasquez padilla ricardo, demirkayagokmen, yogi goswami d, stefanakoselias, rahman muhammad m. heat transfer ananlysis of parabolic trough solarreceiver. Appl energy 2011;88:5097-110.

10. Edenburn michael w. performance analysis of a cylindrical parabolic focusing collector and compression with experimental results. Sol energy 1976;18:437-44.

11. Experimental studies of a double pipe helical heat exchanger, Timothy J. Rennie, Vijaya G.S. Raghavan

12. W. El Maghlany, E. Eid, M.Teamah, L. Shahrour, Experimental study for double pipe heat exchanger with rotating inner pipe, International Journal of Advanced Scientific and Technical Research, issue 2 Vol.4, pp.507 to 524, 2012